LRP 459/92 August 1992

ELECTRON CYCLOTRON RESONANCE HEATING ON THE TCA TOKAMAK

Z.A. Pietrzyk, A. Pochelon, R. Behn,
A. Bondeson, M. Dutch, T.P. Goodman,
M.Q. Tran, D.R. Whaley

submitted for publication in

Nuclear Fusion

Electron Cyclotron Resonance Heating on the TCA Tokamak

Z.A. Pietrzyk, A. Pochelon, R. Behn, A. Bondeson, M. Dutch, T.P. Goodman,
M.Q. Tran, D.R. Whaley

Centre de Recherches en Physique des Plasmas
Association Euratom-Confédération Suisse
Ecole Polytechnique Fédérale de Lausanne
21 av. des Bains, CH-1007 Lausanne Switzerland

Abstract

Electron Cyclotron Resonance Heating experiments at 39 GHz and power levels similar to Ohmic heating power levels have been conducted in the TCA tokamak, in either X- or O-mode. ECRH was observed to be more efficiently absorbed for low density and low q_a discharges. At low density the central electron temperature is increased by a factor of two over Ohmic cases and the stored energy increased by 40% with up to 80% of the plasma energy supplied by ECRH. During ECRH low density operation the electron energy confinement time τ_{Ee} is the same as during pure Ohmic heating but τ_{Ee} degrades with ECRH power at high density. The decrease in the loop voltage required to maintain a constant current during ECRH is a very reproducible quantity and can be attributed in almost all cases to the change in the electron temperature. Sawtooth stabilization was produced with a sawtooth period of up to 10 times greater than that before ECRH. This stabilization depends on the ECRH toroidal injection angle and total input power. High energy ions are observed and their production is attributed to a 3-wave interaction process.

Introduction

Electron Cyclotron Resonance Heating (ECRH) transfers the electromagnetic wave energy directly to the electrons. The absorption occurs near the electron cyclotron resonance and possibly near the upper hybrid resonance for X-mode heating in a low temperature plasma. This technique has been used for plasma heating and/or current drive in several tokamaks [1,2,3]. Power can be deposited at the fundamental frequency or at its harmonics and the theory of heating and current drive is fairly well developed [4,5].

One important aspect of the heating is the access to the plasma by the wave. In this paper we consider X- and O- mode launch at fundamental frequency. Due to the right hand cutoff located to the low field side of the magnetic axis, an X-mode wave can access high densities only from the high field side, that is from the inside of the torus, a scheme which appears problematic in a reactor. For heating this aspect may not be critical, since the wall of the vessel is an almost perfect reflector at these frequencies and hence X-mode waves launched from the low field side will eventually find their way into the plasma [3]. For profile control, however, the location of the energy deposition is lost.

If the electron cyclotron resonance is placed near the magnetic axis, then an X-mode wave launched from the high field side will be partially absorbed at this resonance and the remainder will propagate to the upper hybrid resonance, where it may be reflected and converted to the Bernstein wave. This conversion depends on the toroidal injection angle [5]. The Bernstein wave will be fully absorbed as it propagates back to the electron cyclotron resonance. First-pass absorption at the electron cyclotron resonance depends on the plasma density and temperature. It increases for both X- and O-mode monotonically with temperature and decreases monotonically with density for X-mode and shows a maximum with respect to density for O-mode. With O-mode launch, the non-absorbed power in the first pass will be reflected from the wall of the vessel and redirected into the plasma, possibly with a changed polarisation and injection angle depending on details of the wall. The propagation of the O-mode is limited by the cutoff density at about half the density of the corresponding X-mode cutoff.

In the TCA experiment, the first goal of the ECRH implementation was to study breakdown and wave assisted startup [6]. Plasma heating was also studied and the experimental results will be presented here. The wave was launched from the high field side with the ability to change polarisation from X- to O-mode on a shot to shot basis. We observed the heating both by the central electron temperature rise (local quantity) and by the increased total plasma energy (global quantity). The heating was more efficient at low density, where about 80% of the plasma energy can be attributed to the wave energy. The loop voltage was always reduced during the heating which can be explained in most of the cases by a reduction in plasma resistivity.

It has been observed that ECRH can stabilized the sawteeth oscillations [2,7,8,9]. There are two possible mechanisms for this stabilization, the first is current profile modification [10] and the second is stabilisation by the energetic particles accelerated by the wave [11]. It is possible that both mechanisms are important and their relative importance depends on the specifics of the experiment.

In this experiment the sawtooth period was strongly modified. At high density this modification can be explained by a change in plasma resistivity as in the Kadomtsev model of sawteeth. However, at low density the modification is much stronger than predicted by a change in resistivity and in this range sawteeth are most likely stabilized by energetic particles. Contrary to observations in [9] this stabilisation also takes place when the resonance is located at the magnetic axis.

Target plasma and diagnostics

The target plasma had line-averaged density between (0.6-1.7) $\times 10^{13}$ cm^{-3} with the current ranging from 100 to 120 kA and the safety factor q_a from 3.2 to 4.8. All of the experiments were performed with a boronized wall [12], which allowed for low Z_{eff} and low Ohmic power, with a loop voltage of typically 1.2 V. A toroidal magnetic field of 13.9 kG was used to place the resonance layer at the magnetic axis. In some shots the magnetic field was varied between 11.9 and 16 kG to obtain the best heating position of the resonance layer. A detailed description of the machine can be found in [13].

The ECRH was performed using a 39 GHz gyrotron with injection from the high field side (see Fig.1) for good access in both X- and O-mode operation. X- or O-mode polarisation could be selected between shots and a steering mirror allowed for injection of the beam up to ±25° in the toroidal direction, and poloidally in the upper half plane. The standard launch used was±25° with a poloidal angle chosen to aim at the plasma axis. The gyrotron delivered up to 145 kW of power to the plasma. The power was limited at that time by breakdown in the transmission line at high power. A description of the microwave system can be found in [14].

Standard diagnostics were available on TCA and were recently upgraded by the addition of a single-time, 10-point Thomson scattering system [15].

Heating

1. Profiles

The central diagnostic for determining the ECRH performance was a Thomson scattering system simultaneously measuring spatial profiles of T_e and n_e. A single profile per shot was taken at the end of the ECRH pulse.

As an example of heating, four radial profiles of the plasma electron temperature measured by the Thomson scattering system are shown in Fig. 2. The figure consists of a reference shot with OH heating only, a shot with O-mode heating and two shots with X-mode heating. The value E_e given in the figures represents the total plasma electron energy calculated by

$$E_e = (2\pi)^2 R \int_0^a \frac{3}{2} n_e(r) T_e(r)\, r\, dr \qquad (1)$$

where n_e was taken from the density profile measured by Thomson scattering (Fig. 3) with the line average density calibrated by an FIR interferometer for each shot [15]. All three heated shots show an increase of the central temperature and the total plasma energy. O-mode (42497) and X-mode (42502) heated plasma can result in almost the same temperature profiles, but very peaked T_e profile can also be observed, for example in X-mode (42495). However, such peaked profiles are also observed for O-mode heating.

2. Dependence of heating on initial plasma parameters

The dependence of the central electron temperature and total electron energy on the line-averaged density is shown in Fig. 4. In this figure the data for OH cases are represented by stars and are fitted with the solid straight line shown in the figure. During ECRH the central electron temperature can increase as much as a factor of two over OH cases. The total electron energy for ECRH cases is an increasing function of density, as with pure Ohmic cases, but is generally higher than for the OH cases. Some of the "heated" cases do not show an increase in either the central temperature or the electron energy and the spread of data for constant line- average density is large. This shows either

poor reproducibility of heating or dependence of the heating on an unknown parameter. The heating (both central temperature and total electron energy) is also a weak function of q_a, the temperature increment decreases with increasing q_a.

The poor reproducibility of the heating may be due to the fact that the ECRH waves interact strongly with the energetic electrons in the tail of the distribution. For this reason, if the unheated distribution is slightly non-Maxwellian the heating may be different. The departure from a Maxwellian distribution does not need to be large, as the ECRH wave interacts with electrons in the tail of the distribution [16] and this small departure may be hard to detect experimentally.

3. Heating efficiency

Our Thomson scattering diagnostic provides only a single set of T_e and n_e profiles for each TCA discharge. The total plasma energy increase during ECRH, ΔE_e is estimated by assuming that the plasma energy before heating, $E_e(OH)_{before}$, for a given shot is the same as that of similar pure Ohmic shots at equal density $\bar{n}_e$.

$$\Delta E_e = E_e(OH+ECRH) - E_e(OH)_{before} \qquad (2)$$

The increase in the plasma energy during the ECRH can be characterised by the ratio of the increase in electron energy ΔE_e to the total electron energy E_e before heating. Fig. 5a shows a graph of this ratio, $\Delta E_e/E_{ebefore}$ as a function of line average density. It shows that the total electron energy is up to 40% higher with ECRH and this ratio decreases with density. The amount of energy supplied to the plasma by ECRH is higher than this value, as some of the Ohmic power is replaced by the ECRH power due to a decrease in the required loop voltage to maintain a constant plasma current. Nevertheless, this simple expression (2) is useful as a measure of the energy increase.

The estimated energy increase using this method does not include the OH energy which is replaced by the ECRH, nor the expected changes in transport during the heating. One can say that the energy supplied to the plasma from ECRH is the increase in energy of the plasma during ECRH plus the drop in the energy delivered by OH, which occurs during ECRH. The replaced energy is difficult to calculate precisely but one can make

a rough estimate assuming that the replaced energy is the amount by which the OH power is reduced multiplied by the electron energy confinement time.

$$E_{eECRH}=E_e(OH+ECRH)-E_e(OH)_{before}+\Delta V_l I_p \tau_{Ee} \qquad (3)$$

Here, E_{eECRH} is the total electron energy deposited by ECRH, E_e is the total electron stored energy, V_l is the resistive loop voltage, I_p is the plasma current, and τ_{Ee} is the electron energy confinement time. V_l is calculated as $V_l=U-L_i(dI_p/dt)$ where U is the measured loop voltage. Fig. 5b shows the $\bar{n}_e$ dependence on the ratio of energy from the ECRH to the total electron energy of the plasma. A maximum of about 80% of the plasma energy comes from the ECRH at low density and this ratio decreases with increasing density.

Fig. 6 shows the average energy increase per electron $E_e/\langle n_e \rangle$ as a function of ECRH power and central density. One can see that in the range of parameters investigated for X-mode heating, the average electron energy increases with ECRH power and decreases with central density.

In the above calculations only the electron energy has been considered because the ion energy is difficult to measure precisely and is most likely not much different than before the heating as the calculated equipartition time is much longer than the heating pulse. A three-wave interaction process delivers energy directly to the ions from the ECRH wave (see section about production of fast ions), but this process does not significantly increase the total ion energy .

Energy confinement time.

We have studied the behaviour of the electron energy confinement time at ECRH powers similar to the Ohmic power. We will restrict ourselves to the calculation of the electron energy confinement time only. The information we have about the ion temperature during ECRH is insufficient to make any assumptions about the ion contribution to the energy confinement time. It is reasonable to assume that the bulk of the ions is not heated during the 20 ms ECRH pulse, since the equipartition time for the plasma parameters typical for the ECRH experiment is of the order of 100 ms. Neglecting all of the time dependent terms, the electron energy confinement time can be calculated according to the equation:

$$\tau_{Ee} = \frac{E_e}{(V_l I_p + P_{ECRH})} \qquad (4)$$

where E_e is the total electron energy, V_l is the resistive loop voltage, I_p is the plasma current and P_{ECRH} is the power delivered from the ECRH launcher. The calculated τ_{Ee} is shown in Fig. 7 as a function of $\bar{n}_e$. The data show some degradation of τ_{Ee} with line density for these ECRH powers, compared to the Ohmic heating cases. Usually, it is expected to observe a $P_{tot}^{-0.5}$ dependence. This may be the case for high density discharges in TCA, however, low density degradation of τ_{Ee} with ECRH power is very small, if present. For most of the shots P_{ECRH} was between 90 and 110 kW (with only 2 shots with P_{ECRH} = 145 kW taken at low plasma density). If we plot the X-mode τ_{Ee} data as a power function of $\bar{n}_e$, we obtain $\tau_{Ee} \sim \bar{n}_e^{0.45\pm0.1}$.

Previous scaling of τ_{Ee} with density have shown exponents changes from 0.4 to 1.0 [3,17] for different experiments and the TCA data fall within this range. The scaling with ECRH power is more optimistic here than in [3] at least at low density where τ_{Ee} is the same for ECRH as for an OH plasma. A tentative explanation of this optimistic scaling of τ_{Ee} with ECRH power is the sawtooth stabilisation. Thus, there are two competing effects, the degradation of τ_{Ee} with power and the improvement of τ_{Ee} with sawtooth

stabilisation. As the stabilisation is more efficient at low density, the improvement dominates over degradation, while at high density degradation dominates over improvement. This produces a weak power dependence of τ_{Ee} on density.

Loop voltage decrease and current drive

The most pronounced and reproducible effect observed during ECRH is the decrease in the loop voltage required to maintain a constant plasma current when the ECRH pulse is applied. The loop voltage initially drops rapidly (Fig. 8) during the first 2-3 ms of the ECRH pulse, on a time scale comparable to the energy confinement time. After the initial V_l decrease different types of behaviour can occur; the loop voltage continues to decrease (shot 41522), remains almost constant (shot 42502) or even sightly increases (shot 42447). This kind of behaviour is correlated with the initial drop in the voltage, which is primarily a function of the density $\bar{n}_e$ and the ECRH power, the decrease in V_l being larger for lower density and higher power.

The loop voltage required to maintain a constant current is shown as a function of line-averaged density $\bar{n}_e$ in Fig. 9a. The loop voltage is taken at the end of the ECRH pulse at the time at which the scattering data was taken. The data for X-mode launch and O-mode launch are shown together with data from pure Ohmically heated plasmas. A significant decrease in the loop voltage is visible, particularly for low plasma density. The lower line in this figure is a linear fit to the X-mode data. The values for pure Ohmic heating shots are also shown and are fitted with a straight line. To determine whether the drop in voltage is due to current drive or simply to a decrease in plasma resistivity, a plot of plasma Ohmic resistance $R_\Omega = \frac{U}{I_p} - \frac{L_i}{I_p}\frac{dI_p}{dt} = \frac{V_l}{I_p}$ as a function of $\langle Te^{1.5}\rangle^{-1}$ is shown in Fig. 9b. All of the ECRH data (with the exception of two low resistivity points) lie on the same line as the OH data, with almost the same variance as the OH data. It must therefore be concluded that no significant total current drive was obtained in these experiments except possibly for the low-density, low-resistivity cases. This does not contradict earlier measurements of current drive with the first harmonic launch. [2,18]

Sawtooth period

For Ohmic discharges in TCA, the sawtooth period is a approximately a linear function of density in the range of density from 2 to 5×10^{13} cm^{-3} [19]. Below 2×10^{13} cm^{-3}, the sawtooth period is independent of density. The ECRH experiments were conducted in this low density range, so we can assume that the sawtooth period is not density dependent before ECRH is applied. All of the sawtooth period data presented here were taken with the resonance on the magnetic axis and a toroidal injection angle $\pm 25^{o}$.

In the Kadomtsev's sawtooth model [20], resistive reconnection leads to the sawtooth collapse. If this is the case, the sawtooth period should depend on plasma resistivity. Fig. 10 shows the dependence of the sawtooth period on inverse plasma resistance R^{-1} and $\langle T_e^{1.5} \rangle$, which are both measurements of inverse plasma resistivity, assumed to be classical. R^{-1} is obtained directly from the resistive loop voltage and the measured plasma current and $\langle T_e^{1.5} \rangle$ from the Thomson scattering measurements. Data for Ohmic, X-mode and O-mode injection are shown. Most of the data points lie close to a straight line, as expected if resistive reconnection is solely responsible for the sawteeth oscillations.

Four of the points are far above the line $\tau_{Ee} \sim \langle T_e^{1.5} \rangle$. All of these four points are taken at very low density 5.8 to 6.8×10^{12} cm^{-3}. In all four cases run away electrons were present even before ECRH. The four data points are for shots with different conditions. Both the ECRH power and the toroidal injection angle were varied. Two of these shots (longest sawteeth) are for higher (145 kW) ECRH power and opposite toroidal injection angles; one point is in the positive and the other in the negative OH electron drift direction ($\pm 25^{o}$). The other two are for lower ECRH power (110 kW) and also two opposite toroidal injection angles. The trend appears to be that higher ECRH power and the injection opposite to the electron drift direction is favourable for the stabilization of the sawteeth. Although the exact mechanism for the stabilization is not clear, the generation of a population of hot trapped ions [11] is a likely candidate. Previous suggestions that the

presence of runaway electrons stabilizes the sawteeth [19] do not seem to apply here, since the same amount of hard x-rays was observed for ordinary shots as for those with stabilized sawteeth. It seems that for efficient stabilization of sawteeth the plasma should be at low density but not necessarily at low pressure. In fact, the sawtooth period is longest for low density shots where a large increase in plasma pressure is observed. The dependence on toroidal injection angle could be related to the associated changes in the power deposition profile in the plasma.

The sawtooth period increased during ECRH in some cases by as much as a factor of ten. Fig. 11 shows an example of soft x-ray traces before, during and after ECRH. In this shot one can see the increase in the sawtooth period by about a factor of two during ECRH (125-145 ms), over the OH part of the discharge, without a significant change in the inversion radius position. Fig. 12 shows an example of the central x-ray channel for the case when sawtooth period during ECRH increased 10 times over the period before when ECRH was applied. As in Fig. 11, the inversion radius for the shot did not change.

We have tried several empirical scaling of the sawtooth period with experimental parameters. The best correlation for the sawtooth period is found with $P_{tot}/\langle n_e \rangle$ (the total power per particle), which is shown in Fig. 13. This suggests a stabilization by energetic particles, although the evidence is not sufficient.

The instability responsible for the sawtooth crash has been studied by means of magnetic probes placed in the limiter shadow of large, low-aspect-ratio tokamaks [21]. In smaller, Ohmically-heated tokamaks, the magnetic signal associated with sawtooth crashes are usually below the noise level. However, with the addition of central ECRH close to the Ohmic power level (P_{ECRH} = 110 kW), the magnetic perturbation associated with the temperature crash became measurable in TCA. It was Fourier analyzed with eight probes equally spaced along the toroidal direction on TCA, yielding the n = 0, 1, 2, 3 toroidal components. The amplitude of the n = 1 component (a non-local quantity) and the associated sawteeth crash amplitude measured on the soft x-rays (a local quantity) are shown proportional in Fig. 14a as in [21]. There is an pronounced n = 1 component of the magnetic signal at the time of the sawteeth crash. The growth time of this component is typically 20 μs. The correspondence between the level of the magnetic pulse at the edge

and the relative crash amplitude in the centre is shown in Fig.14b. The extrapolated Ohmic crash amplitude $\Delta SX(0)$ is 0.08 - 0.10 a.u. would give an $n = 1$ component below the level of detectability (~0.2 a.u.) set by the presence of magnetic turbulence. From Fig. 14a, the ratio of the $n = 2$ to $n = 1$ component is smaller than or equal to 20%. These data give an indication of the m-spectrum on $q = 1$ surface (as $m/n = q = 1$). Self consistent numerical simulation [22] of the sawtooth activities also predict substantially lower amplitude of the higher mode numbers.

Density reduction

It has been observed elsewhere, e.g. [2], that during ECRH the line average density decreases, a phenomenon usually called "pump-out". Ref. [2] suggests that this is not really a loss of the particles from the plasma but a modification of the density profile. In our experiment the line-averaged density was controlled by a feedback system. Because of the finite time response of the feedback system the density changes slightly during ECRH. The compensation action of the gas valve must be taken into account when interpreting the density decrease that has been observed during ECRH. Fig. 15 shows the time dependence of the density for typical cases during ECRH. The general trend is that for low density there is no density decrease during the ECRH interaction and there is no increase in the gas valve flux. At high density, a decrease of density exists and the increase in the gas flux injected into the plasma can be as high as 3 times the flux before ECRH. Fig. 16 shows the relative drop of the line average density and the gas valve flux increase as a function of the line average density. For low density there is no density reduction due to ECRH, but for large density the effect becomes substantial.

Production of Fast Ions

The production of energetic ions during the ECRH pulse has been observed with a neutral particle analyser (NPA) used to measure the ion temperature on TCA. Although there are no direct measurements of bulk ion temperature from the plasma centre it is believed that the bulk ion temperature does not change during ECRH. The NPA signals, however, with lowest channel at 750 eV, change significantly. The ion temperature before and after ECRH injection is approximately 200 eV and the bulk temperature most likely remains the same during ECRH, while the high energy tail shows the "temperature" about 500 eV during ECRH.

Fig. 17 clearly indicates the production of a fast ion tail during ECRH. This tail is produced very soon after the start of ECRH injection (less than 600 μs). This fast rise of a hot ion population indicates that it cannot be the result of a bulk ion temperature increase, but rather an increase in the tail of the distribution. The magnitude of the effect is considerably larger for X-mode launch than for O-mode launch and the effect is also strongest at low plasma densities. The production of fast ions during ECRH has been previously seen on other tokamaks, notably Versator II [23] and FT1 [24] and is attributed [23] to 3-wave parametric decay of the extraordinary wave into a lower-hybrid and an electron Bernstein wave at the upper hybrid resonance layer. The presence of a smaller, but measurable effect with pure O-mode launch specially at low density is most likely due to incomplete first-pass absorption and partial conversion to X-mode upon reflection from the vacuum vessel walls.

Conclusions

The TCA ECRH experiment was conducted at ECRH powers similar to standard Ohmic powers at the fundamental frequency in both X- and O-mode. The central electron temperature increases by as much as a factor of two over pure Ohmic discharges at low density. The total electron energy increases by over 40% for the same cases. The ECRH heating power level at the start of the pulse was close to the Ohmic values, but at low density shots the heating power reached a level above a factor of 3 higher than the instantaneous Ohmic power due to the decrease of the OH power during the ECRH pulse.

Several interesting properties of the ECRH plasma have been observed in this experiment.

The fraction of power supplied to the plasma by ECRH (including the OH power replaced by ECRH) is about 80% of the total power for low density, but this percentage decreases with increasing line-averaged density.

At the power levels used in our experiment, the electron energy confinement time does not show a degradation with power at low plasma density, but we observed that with ECRH injection the energy confinement time becomes only a weak function of density. At higher densities the expected degradation of the energy confinement time is clearly visible.

The decrease in the electron density during ECRH (pump-out) is large at high line-averaged densities, but is completely absent at low density where we observed a large temperature increase.

Sawtooth stabilisation is observed, with the sawtooth period increasing by up to factor of 10 over unheated cases. This stabilisation is strongest at low density and high heating power and is most likely due to the fast particles generated during the heating.

The magnetic signal at the vacuum vessel wall related to the sawtooth crash - the so-called "gong" - has been observed . It shows a dominant n=1 component during sawtooth crash which is too small to be observed in OH discharges in TCA. The n=2 component amplitude is lower than 20% of the n=1 component.

The production of a high-energy ion tail during ECRH has been observed with the NPA ion temperature diagnostic. This effect is greater for X-mode launch and for low plasma density.

Acknowledgments

This work was partially supported by the Swiss National Science Foundation.

References

1. ALIKAEV, V.V., ARSENTIEV, Yu. L., BAGDASAROV, A.A., et al., Plasma Phys. and Contr. Nuclear Fusion Research **1** (1984) 419

2. TFR GROUP, Nuclear Fusion, **28** (1988) 1995

3. STALLARD, B.W., CONTENT, D.A., GROEBNER, R.J., et al., Nuclear Fusion **30** (1990) 2235

4. GOLANT, V.E., FEDOROV, V.I., RF Plasma Heating in Toroidal Devices, Plenum Publishing Corp. (1989) 93

5. BORNATICI, M., CANO, R., DEBARBIERI, O., ENGELMANN, F., Nuclear Fusion **23** (1983) 1153

6. WHALEY, D.R., GOODMAN, T.P., POCHELON, A., et al. Nuclear Fusion **32** (1992) 757

7. BOBROVSKII, G.A., ESIPCHUK, Yu.V., SAVRUKHIN, P.V., Fiz. Plazmy 13 (1987) J. Plasma Phys. **13** (1987) 665

8. TERUMICHI, Y., et al., Proc. 8th Int. Conf. on RF Power in Plasma, Irvine (1989) 88

9. HANADA, K., TANAKA, H., IIDA, M., et al., Phys. Rev. Lett. **66** (1991) 1974

10. SOLTWISCH, H., STODIEK, W., MANICKAM, J., SCHLÜTER, J., Proc. of 10th Inter. Conf. on Plasma Phys. and Controlled Nuclear Fusion Research IAEA Kyoto **1** (1986) 263

11. WHITE, R.B., RUTHERFORD, P.H., COLESTOCK, P., et al. Phys. Rev. Lett. **60** (1988) 2038

12. HOLLENSTEIN, CH., DUVAL, B.P., DUDOK DE WIT, T., et al., J. Nuclear Materials **176&177** (1990) 343

13. DE CHAMBRIER, A., COLLINS, G.A., HOLLENSTEIN, CH., et al., "Target Plasma Conditions in TCA" CRPP report LRP 241/84 and CHEETHAM, A.D.,

HEYM, A., HOFMANN, F., et al., 11th Symposium on Fusion Technology, Oxford (1980)

14. POCHELON, A., GOODMAN, T.P., WHALEY, D.R., et al., in Fusion Technology (Proc. 16th Sym. on Fusion Tech. London 1990) Elsevier Science Pub. (1991) 1075

15. PIETRZYK, Z.A., POCHELON, A., BEHN, R., et al., Nuclear Fusion (1992) submitted for publication.

16. ASHRAF, M., BARNSLEY, R., DELIYANAKIS, N., et al., 12th IAEA Conf. on Plasma Phys. and Contr. Nuclear Fusion Research Nice **1** (1988) 541

17. ALIKAEV, V.V., BAGDASAROV, A.A., VASIN, N.L., et al., Sov. J. Plasma Phys. **13** (1987) 1

18. POLMAN, R.W., LOK, J., ROMMERS, J.H., et al., in Radiofrequency Heating and Current Drive of Fusion Devices. Brussels (1992) 321

19. SIMM, C.W., *Etude comparative des disruptions internes avec chauffage additionnel par ondes d'Alvén, dans le plasma du Tokamak TCA.* LRP 334/87 (1987)

20. KADOMTSEV, B.B., Sov. J . Plasma Phys. 1 (1975) 389

21. DUPERREX, P.A, POCHELON, A., EDWARDS, A. and SNIPES, J.S. Nuclear Fusion **32** (1992) 1161.

22. VLAD, G., BONDESON, A., Nuclear Fusion **29** (1989) 1139

23. McDERMOTT, F.S., BEKEFI, G., HACKETT, K.E., et. al., Phys. Fluids **25** (1982) 1488

24. BULYGINSKY, D.G., GUSEV, V.K., DJACHENKO, V.V., et. al., 11th EPS Aachen vol. 7D part I (1983) 457

Figure Captions

Fig. 1. Poloidal cross section of TCA showing the waveguide, quartz window and steering mirror. The accessible poloidal range for the axis of the beam is limited to the region between the hatched zones.

Fig.2. Radial temperature profiles for representative shots. (a) shot 42496 pure Ohmic heating, (b) shot 42497 O-mode heating, (c) shot 42502 X-mode heating broad profile and (d) shot 42495 X-mode peaked profile for $P_{ECRH} \approx 110$ kW.

Fig. 3. Radial density profiles for representative shots. Same shots as in Fig. 2.

Fig.4. (a) Central electron temperature and (b) total electron energy as a function of line-averaged density for P_{ECRH}=90-145 kW. Straight lines are fits to the OH data.

Fig. 5. (a) Ratio of the increase in total electron energy during the ECRH to the total electron energy before ECRH, (b) ration of energy supplied by ECRH to total electron energy during ECRH pulse as a function of line-averaged density. Straight line is a fit to X-mode data.

Fig. 6. Electron energy per particle as a function of (a) ECRH power and (b) central electron density. Critical densities are indicated for X- and O- mode operation.

Fig. 7. Electron energy confinement time as a function of line-averaged density. Straight line is a fit to OH data, while power function is a fit to X-mode data.

Fig. 8. Loop voltage as a function of time for ECRH heating at different densities shot 42447 $\bar{n}_e=1.42\times10^{13}$ cm^{-3}, 42502 $\bar{n}_e=1.15\times10^{13}$ cm^{-3} and 41522 $\bar{n}_e=0.675\times10^{13}$ cm^{-3} X-mode operation.

Fig. 9. (a) Loop voltage as a function of line-averaged density for X-mode, O-mode and pure OH shots. (b) Plasma resistance calculated from the loop voltage and total current as a function of $\langle T_e^{1.5}\rangle^{-1}$.

Fig. 10. Sawtooth period as a function of (a) conductivity R^{-1} and (b) $\langle T_e^{1.5}\rangle$.

Fig. 11. Soft x-ray traces at different radial positions for shot 42495 during ECRH. The"y" axis is a normalised soft x-ray amplitude with the axis shifted for each trace.

Fig. 12. A central soft x-ray trace for shot 41522 during ECRH. The sawtooth period increased 10 times over sawtooth period before ECRH in this experiment.

Fig. 13. Sawtooth period as a function of total power per particle.

Fig. 14. (a) Amplitude of the central soft x-ray channel and two of the toroidal Fourier components of the magnetic oscillation at the edge (n=1 and n=2) versus time near the sawtooth crash and (b) n=1 "gong" amplitude versus soft x-ray signal drop.

Fig. 15. (a) Line average density and (b) gas flux to the vacuum chamber as a function of time for 4 of varying density shots. t=0 at the ECRH start.

Fig. 16. Relative increase in (a) density and (b) gas flux for various X-mode and O-mode shots as a function of line-averaged density.

Fig. 17. Ion tail energy distribution measured with a neutral particle analyser for (a) X-mode injection and (b) O-mode injection.

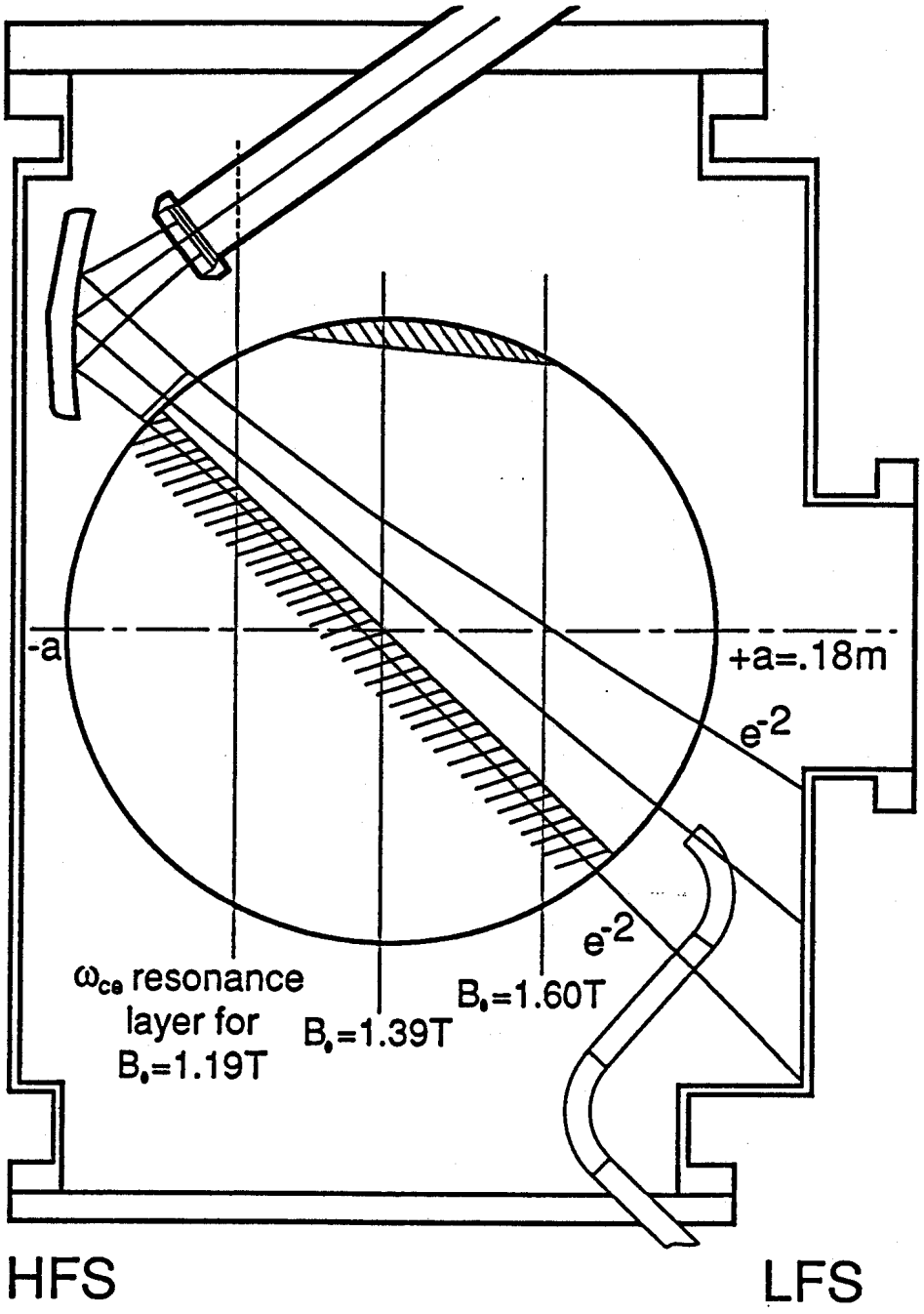
-a
+a=.18m
e-2
e-2
ωce resonance
layer for
Bφ=1.19T
Bφ=1.39T
Bφ=1.60T
HFS
LFS

Figure 1

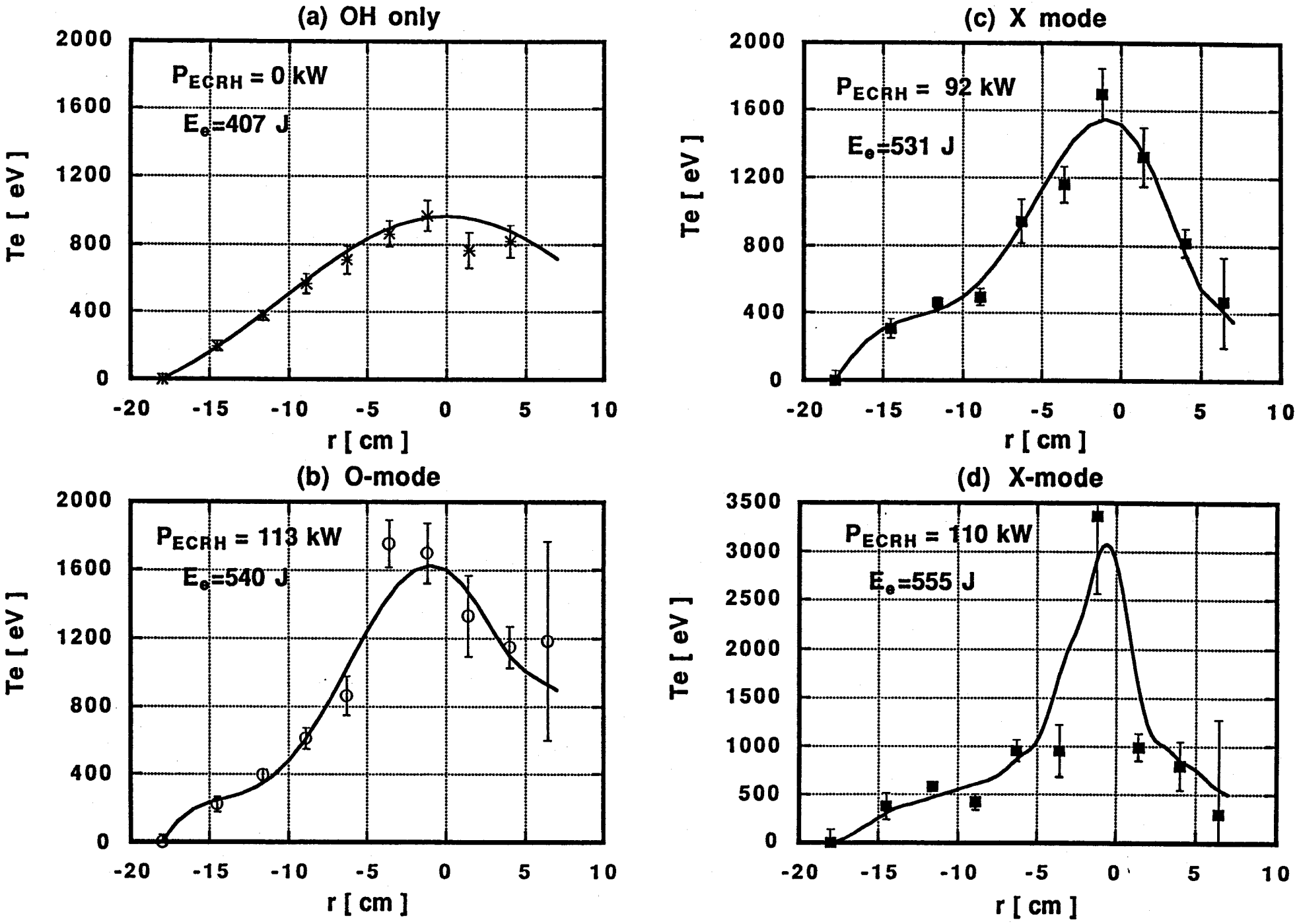
(a) OH only
P_{ECRH} = 0 kW
E_e=407 J
(c) X mode
P_{ECRH} = 92 kW
E_e=531 J
(b) O-mode
P_{ECRH} = 113 kW
E_e=540 J
(d) X-mode
P_{ECRH} = 110 kW
E_e=555 J
Te [eV]
r [cm]

Figure 2

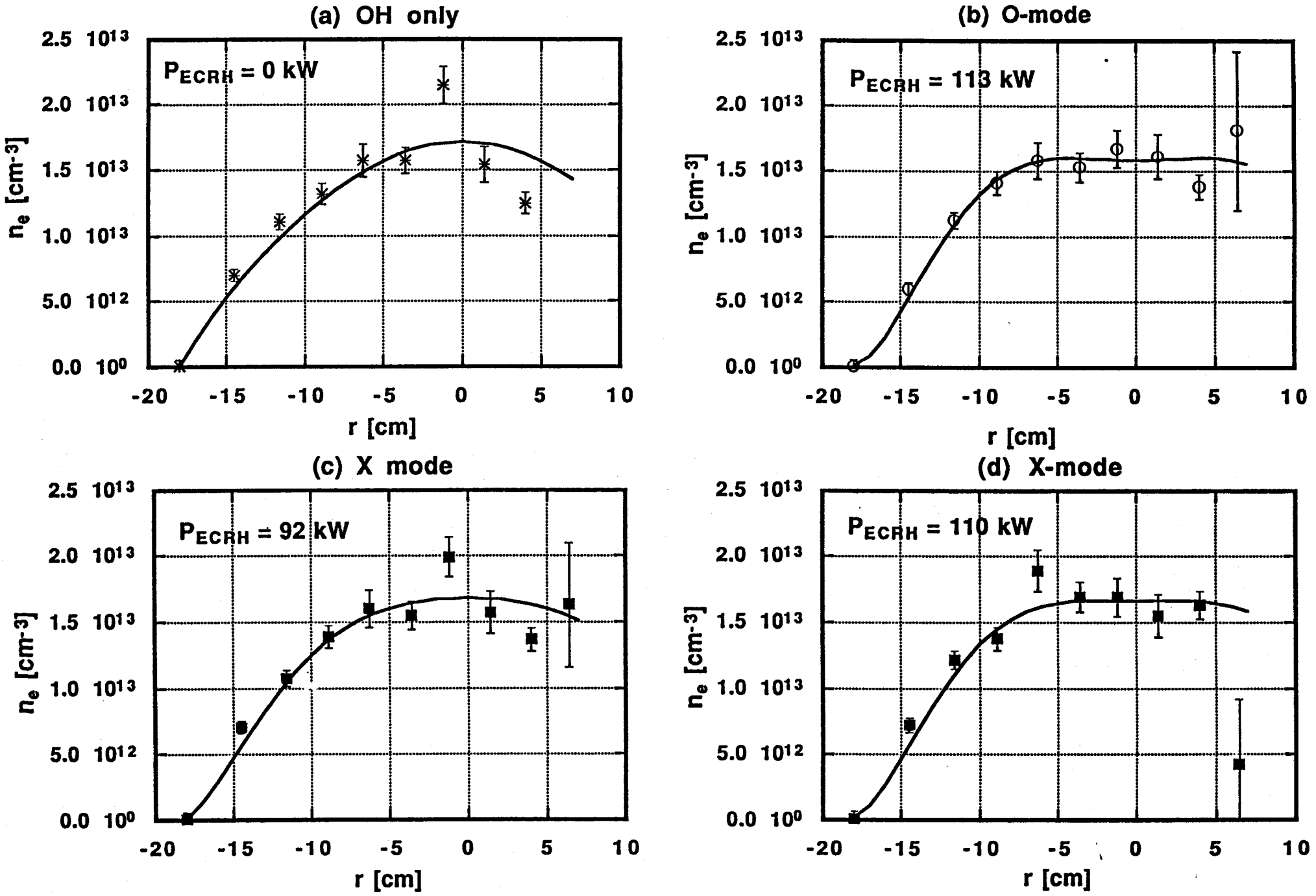
(a) OH only
P_{ECRH} = 0 kW
(b) O-mode
P_{ECRH} = 113 kW
(c) X mode
P_{ECRH} = 92 kW
(d) X-mode
P_{ECRH} = 110 kW
n_e [cm^{-3}]
2.5 10^{13}
2.0 10^{13}
1.5 10^{13}
1.0 10^{13}
5.0 10^{12}
0.0 10^{0}
-20 -15 -10 -5 0 5 10
r [cm]

Figure 3

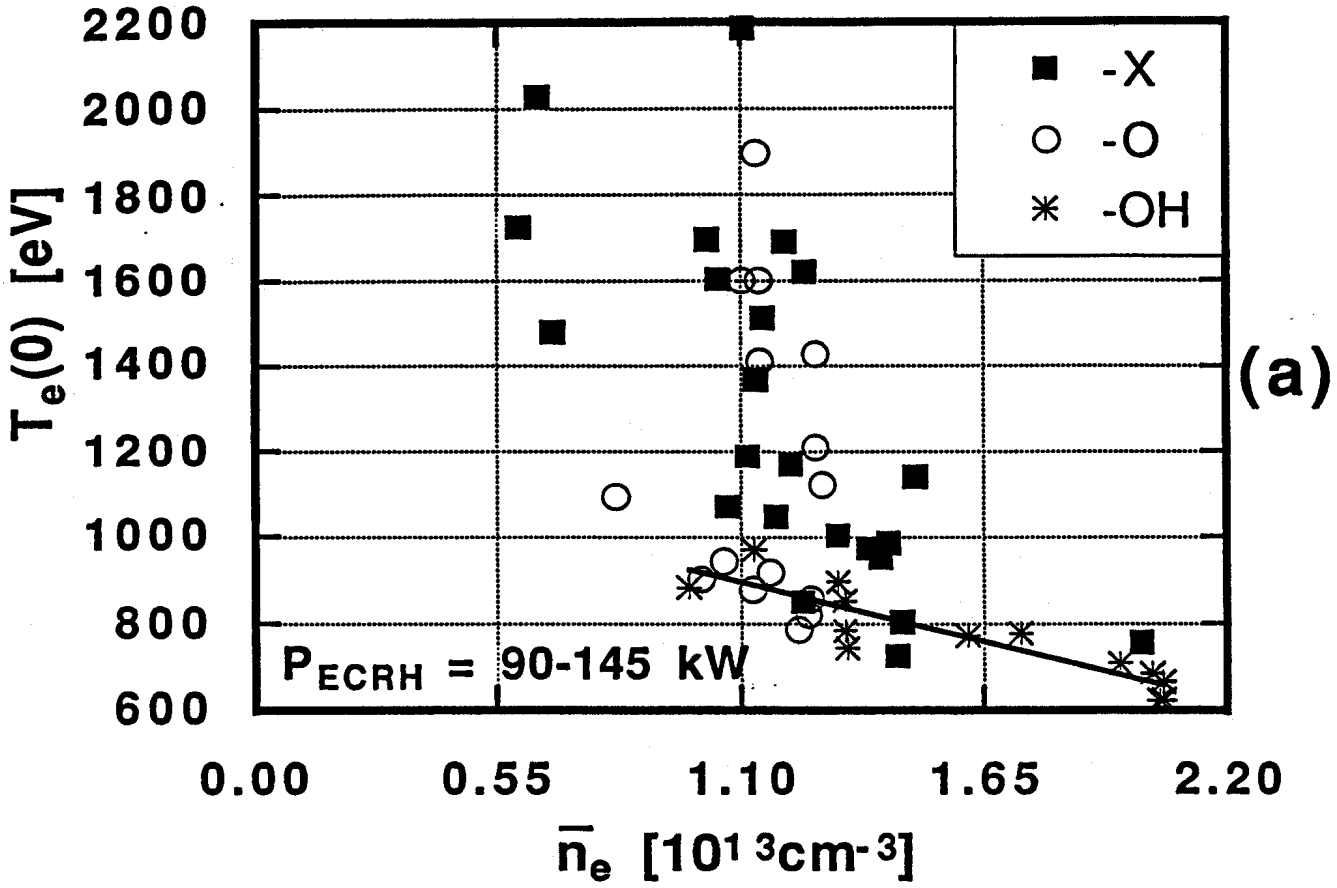
2200
2000
1800
1600
1400
1200
1000
800
600
$T_e(0)$ [eV]
-X
-O
-OH
P_{ECRH} = 90-145 kW
(a)
0.00
0.55
1.10
1.65
2.20
$\bar{n}_e$ [10^{13}cm^{-3}]

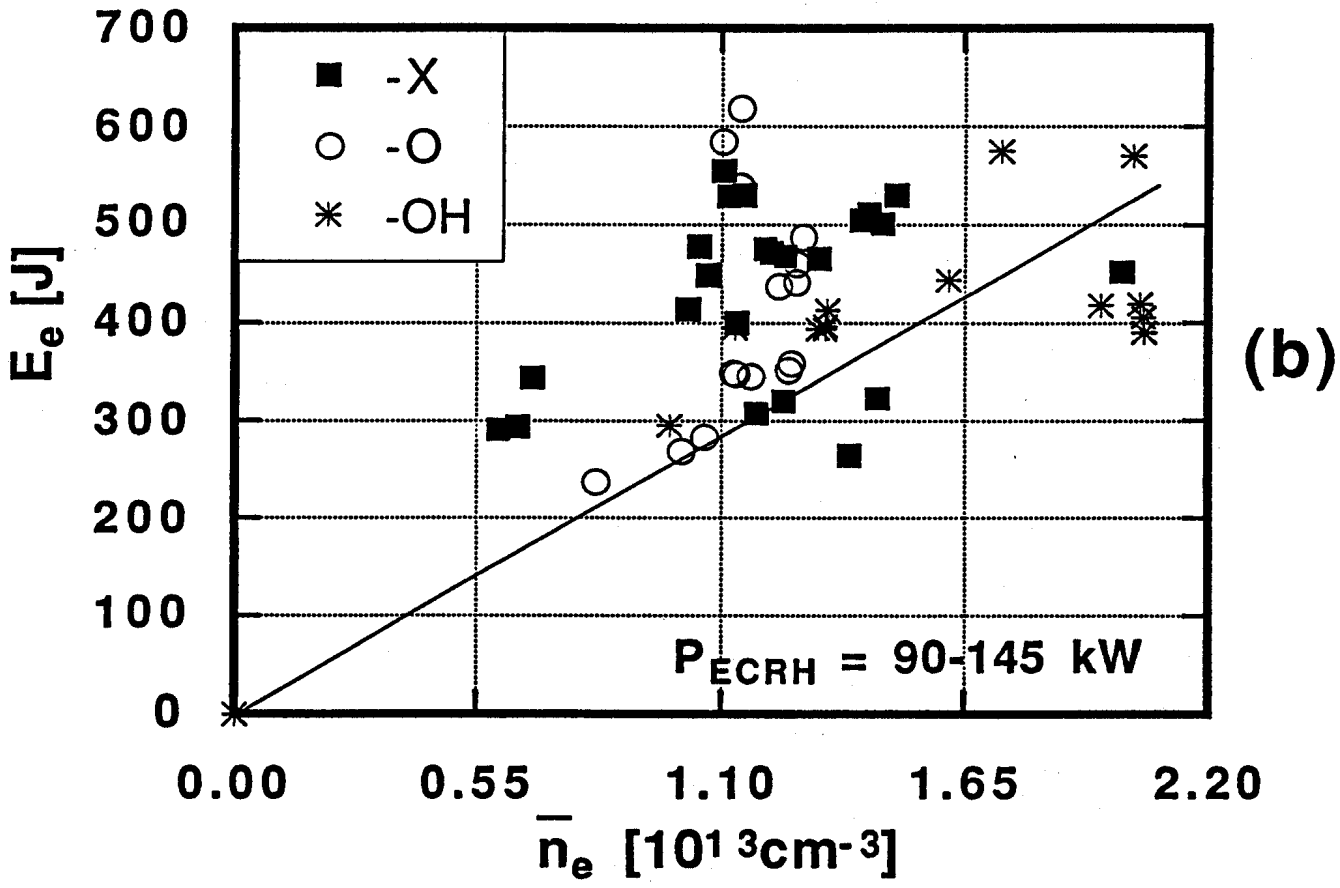
700
600
500
400
300
200
100
0
E_e [J]
-X
-O
-OH
P_{ECRH} = 90-145 kW
(b)
0.00
0.55
1.10
1.65
2.20
$\bar{n}_e$ [10^{13}cm^{-3}]

Figure 4

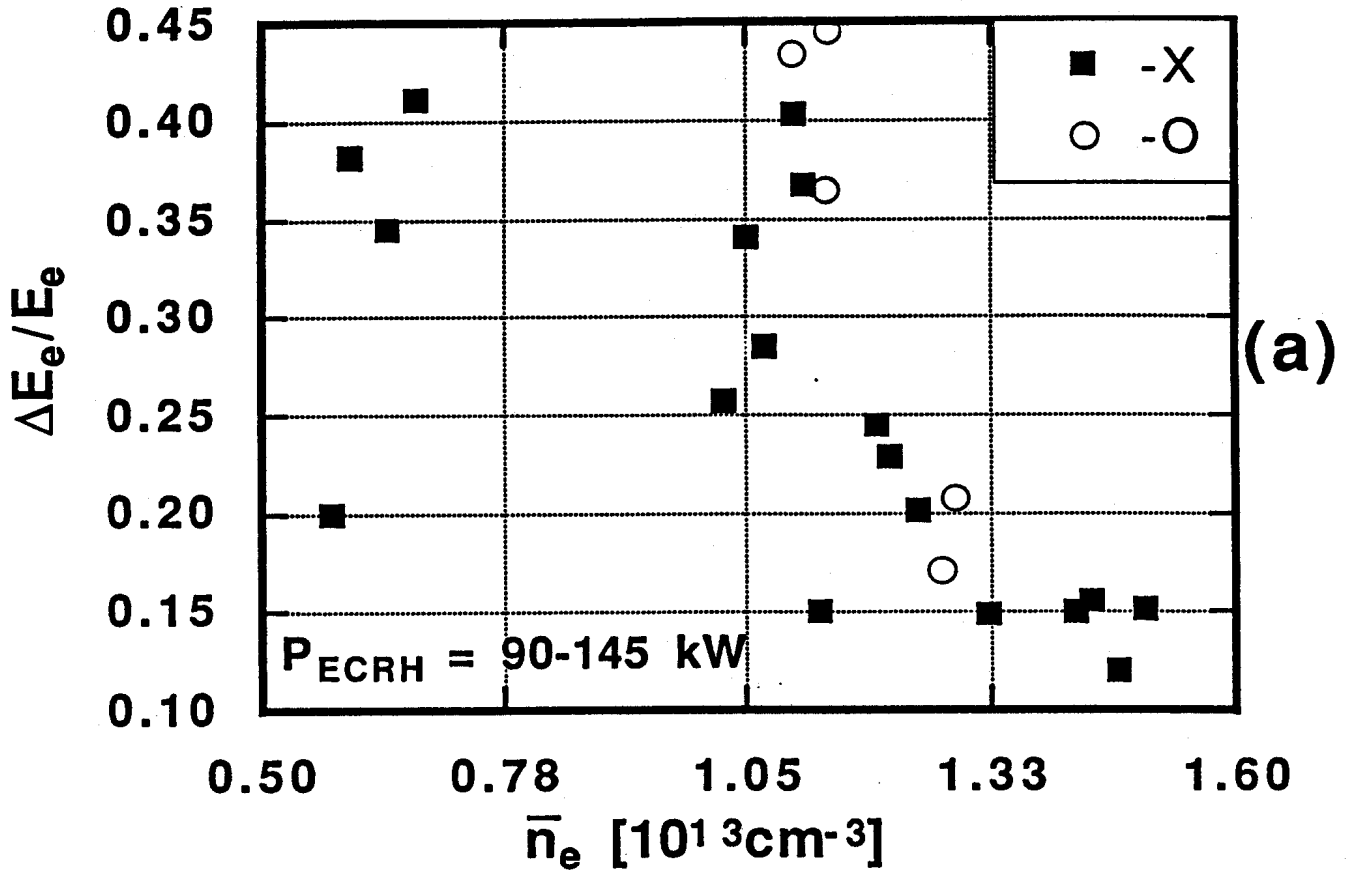
0.45
0.40
0.35
0.30
0.25
0.20
0.15
0.10
ΔEe/Ee
-X
-O
(a)
PECRH = 90-145 kW
0.50
0.78
1.05
1.33
1.60
ne [10¹³cm⁻³]

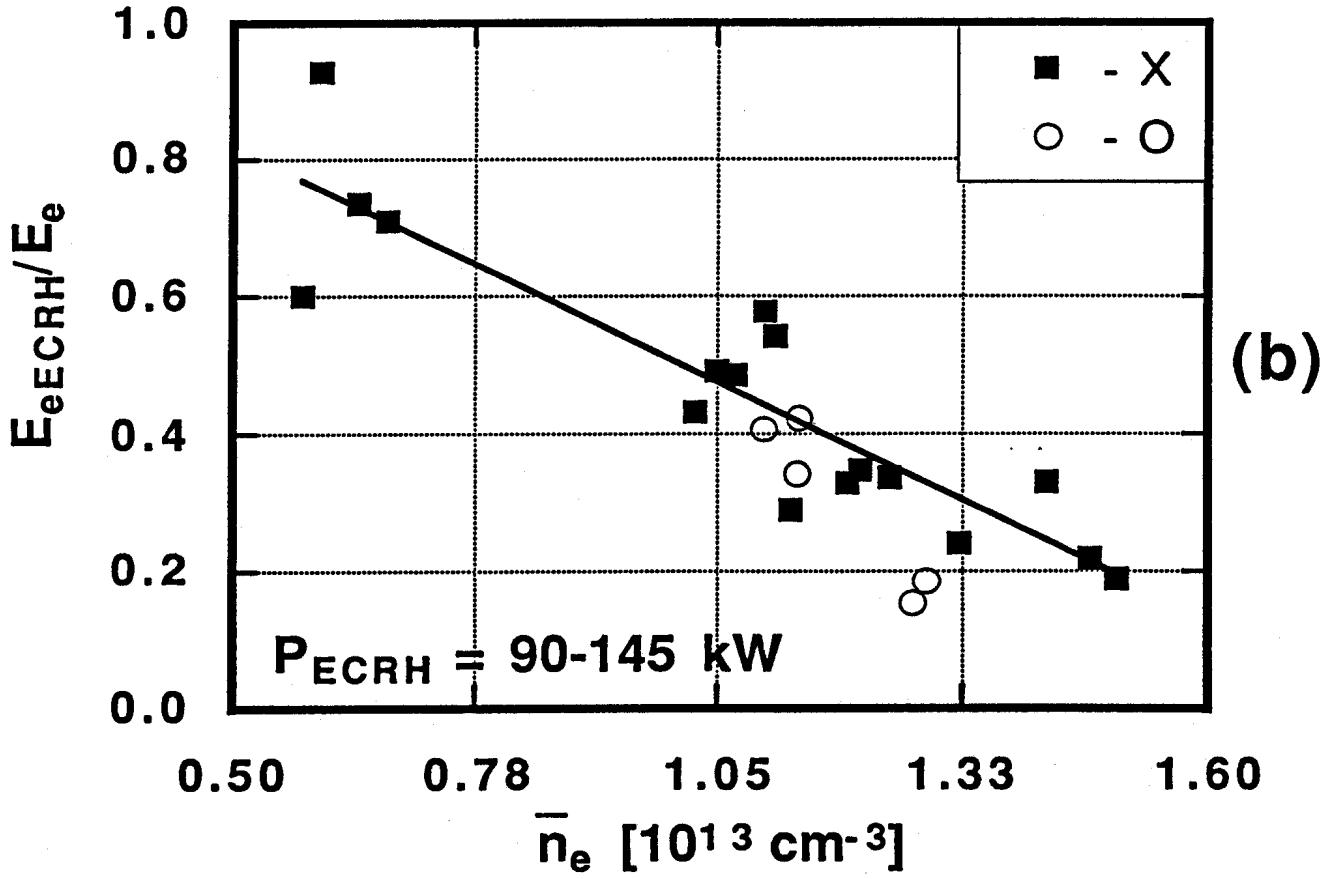
1.0
0.8
0.6
0.4
0.2
0.0
EeECRH/Ee
- X
- O
(b)
PECRH = 90-145 kW
0.50
0.78
1.05
1.33
1.60
ne [10¹³ cm⁻³]

Figure 5

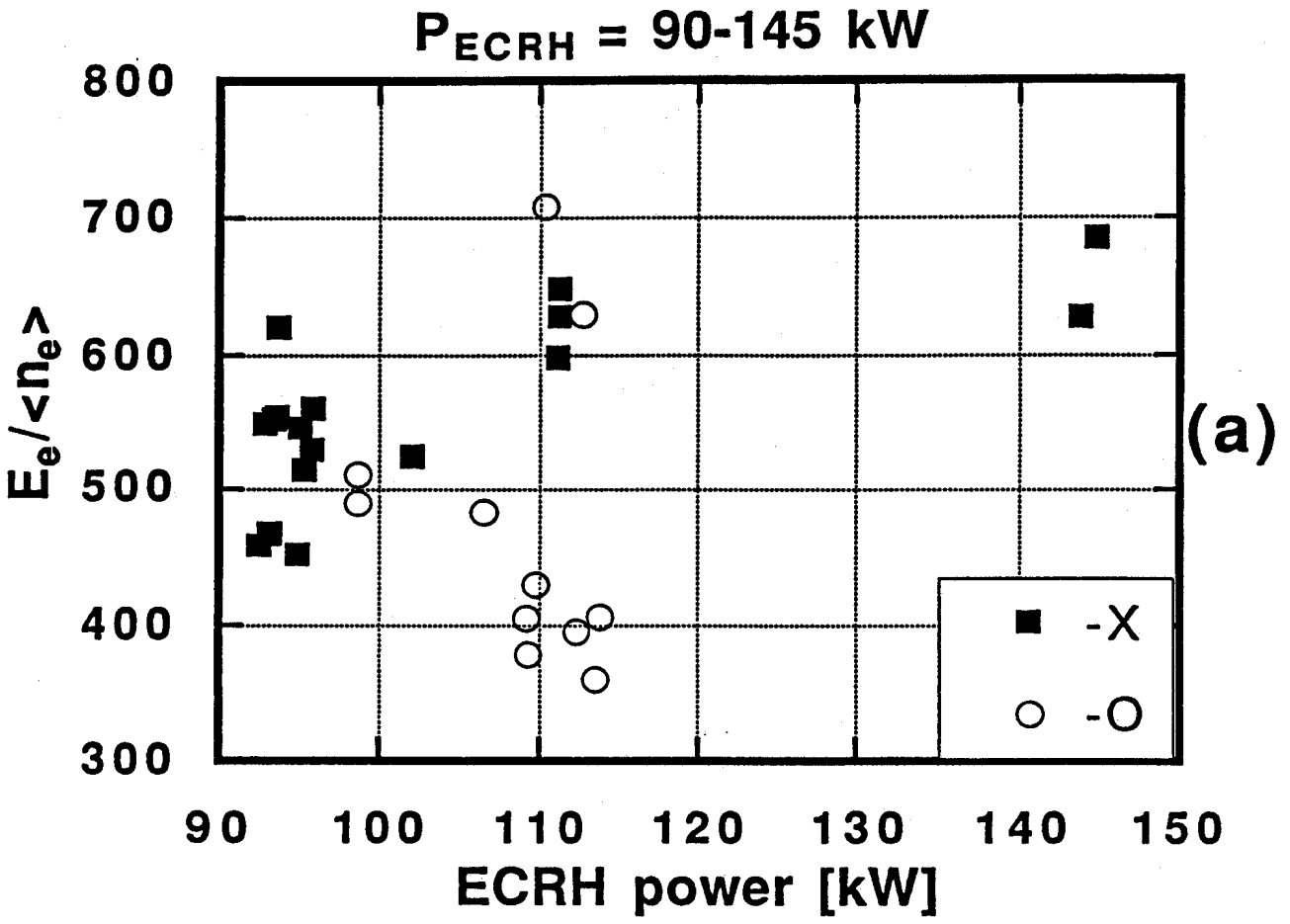
P_{ECRH} = 90-145 kW
800
700
600
500
400
300
$E_e/<n_e>$
(a)
-X
-O
90
100
110
120
130
140
150
ECRH power [kW]

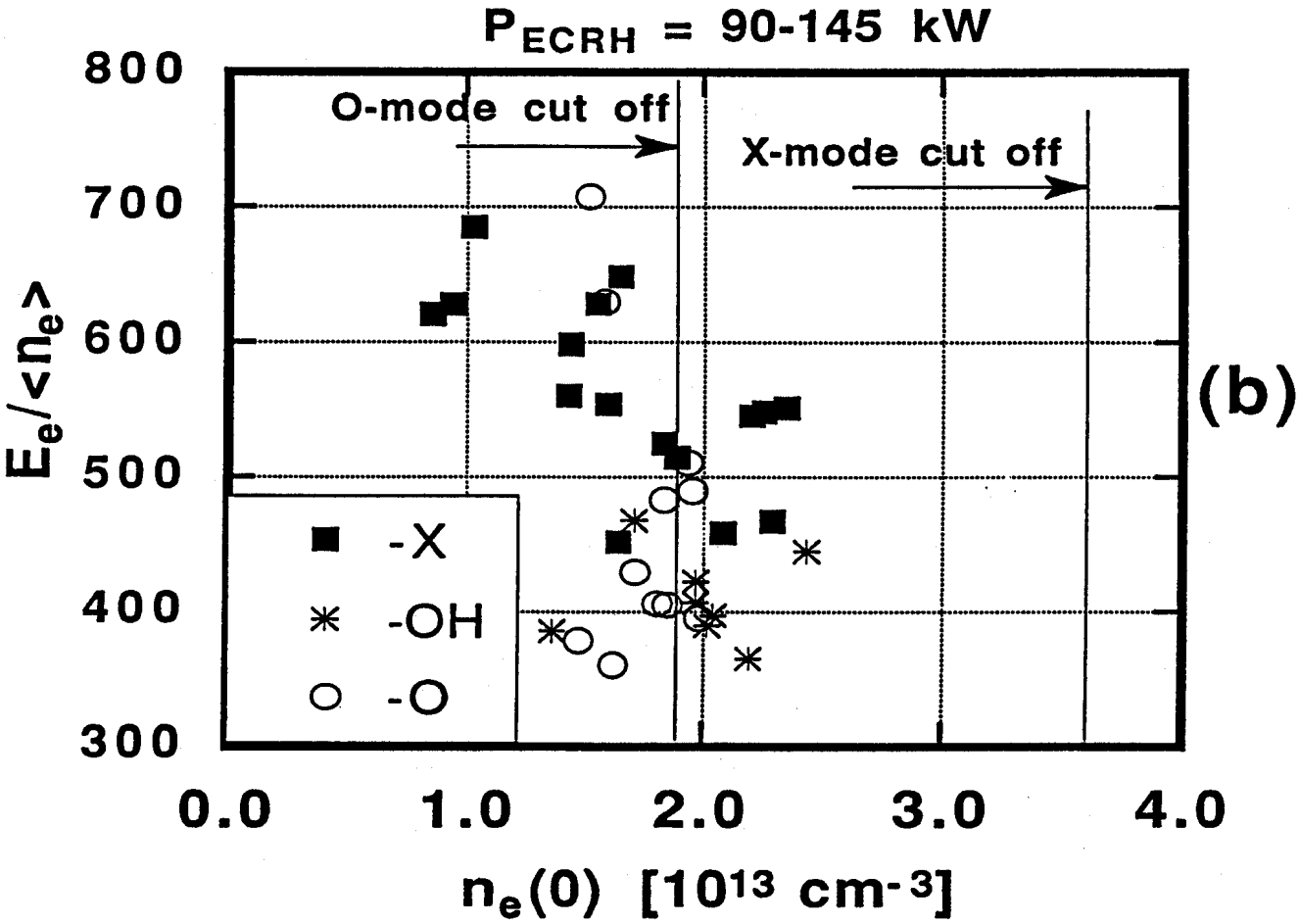
P_{ECRH} = 90-145 kW
O-mode cut off
X-mode cut off
800
700
600
500
400
300
$E_e/<n_e>$
(b)
-X
-OH
-O
0.0
1.0
2.0
3.0
4.0
$n_e(0)$ [10^{13} cm^{-3}]

Figure 6

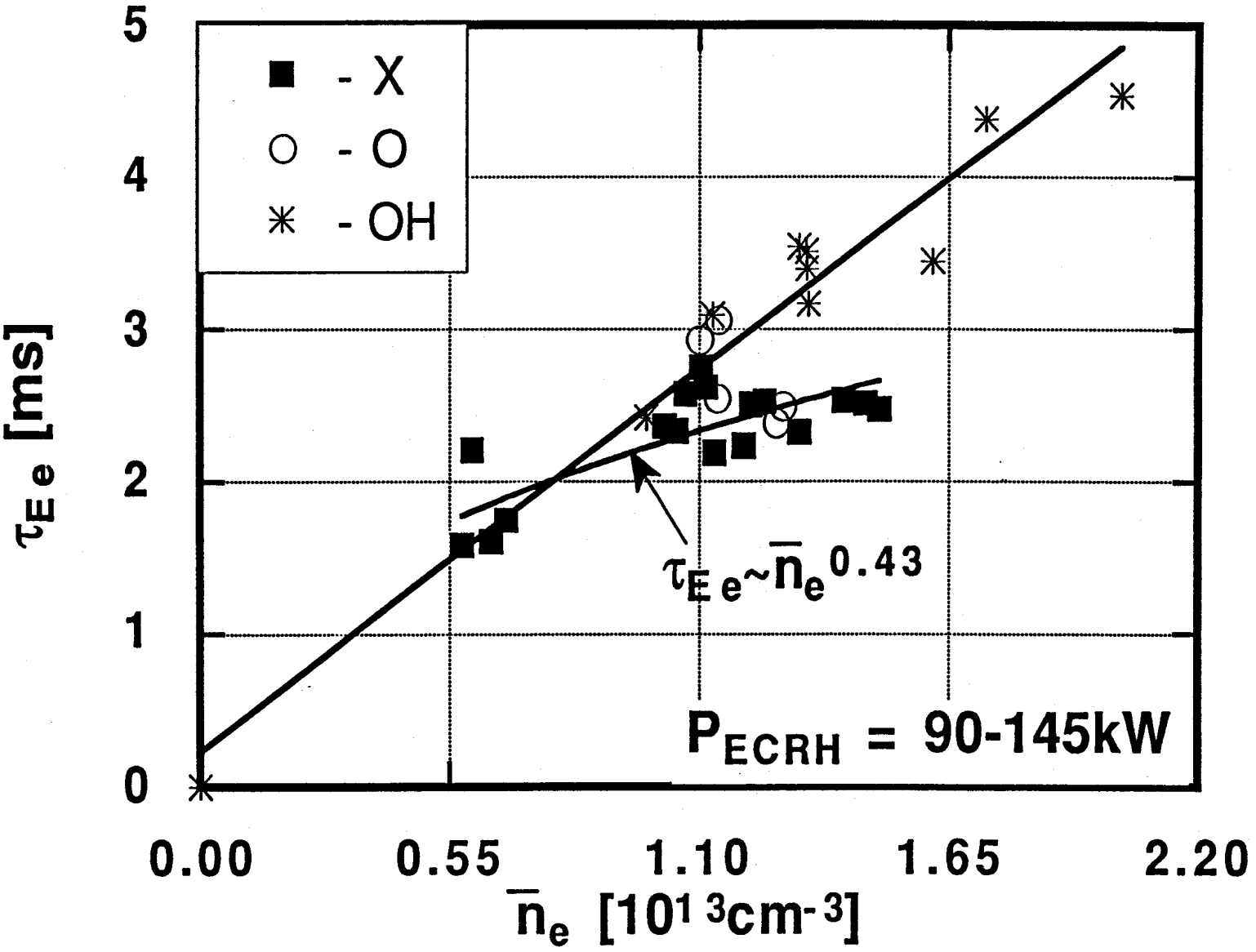
■ - X
○ - O
✳ - OH
$\tau_{E\,e} \sim \bar{n}_e^{0.43}$
P_{ECRH} = 90-145kW
$\tau_{E\,e}$ [ms]
$\bar{n}_e$ [10^{13}cm^{-3}]
0
1
2
3
4
5
0.00
0.55
1.10
1.65
2.20

Figure 7

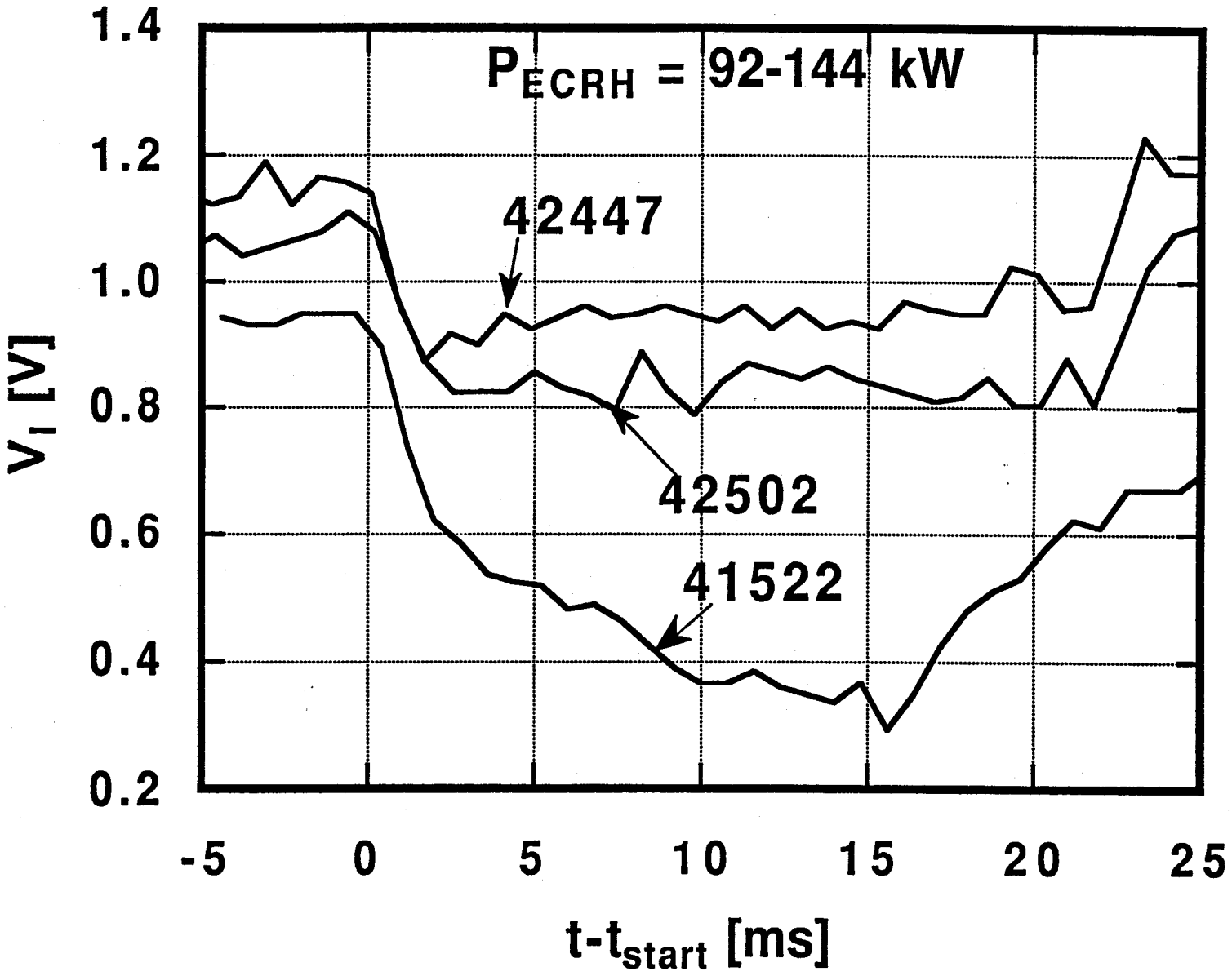
P_{ECRH} = 92-144 kW
42447
42502
41522
V_l [V]
1.4
1.2
1.0
0.8
0.6
0.4
0.2
-5
0
5
10
15
20
25
t-t_{start} [ms]

Figure 8

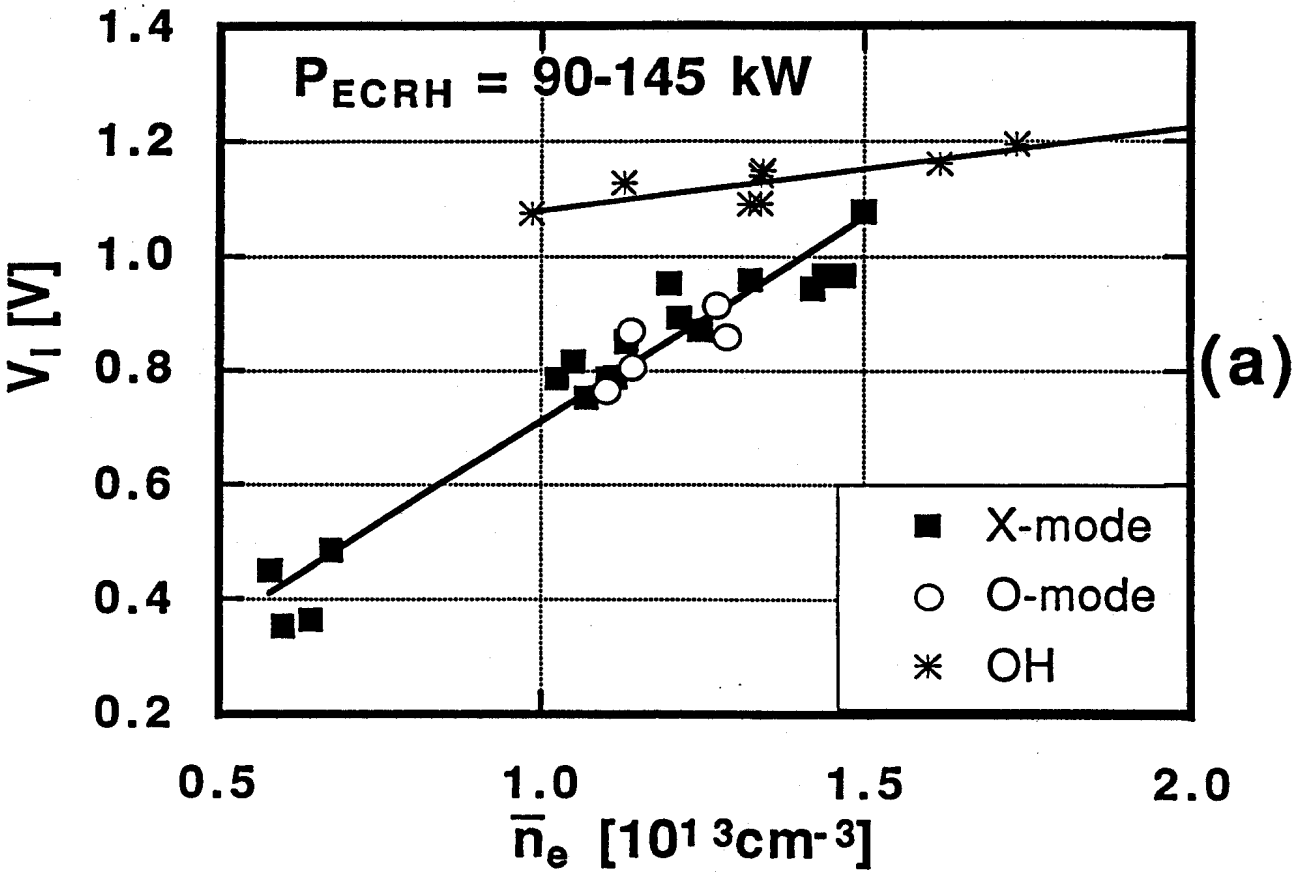
1.4
1.2
1.0
0.8
0.6
0.4
0.2
V_l [V]
P_{ECRH} = 90-145 kW
X-mode
O-mode
OH
(a)
0.5
1.0
1.5
2.0
$\bar{n}_e$ [10^{13}cm^{-3}]

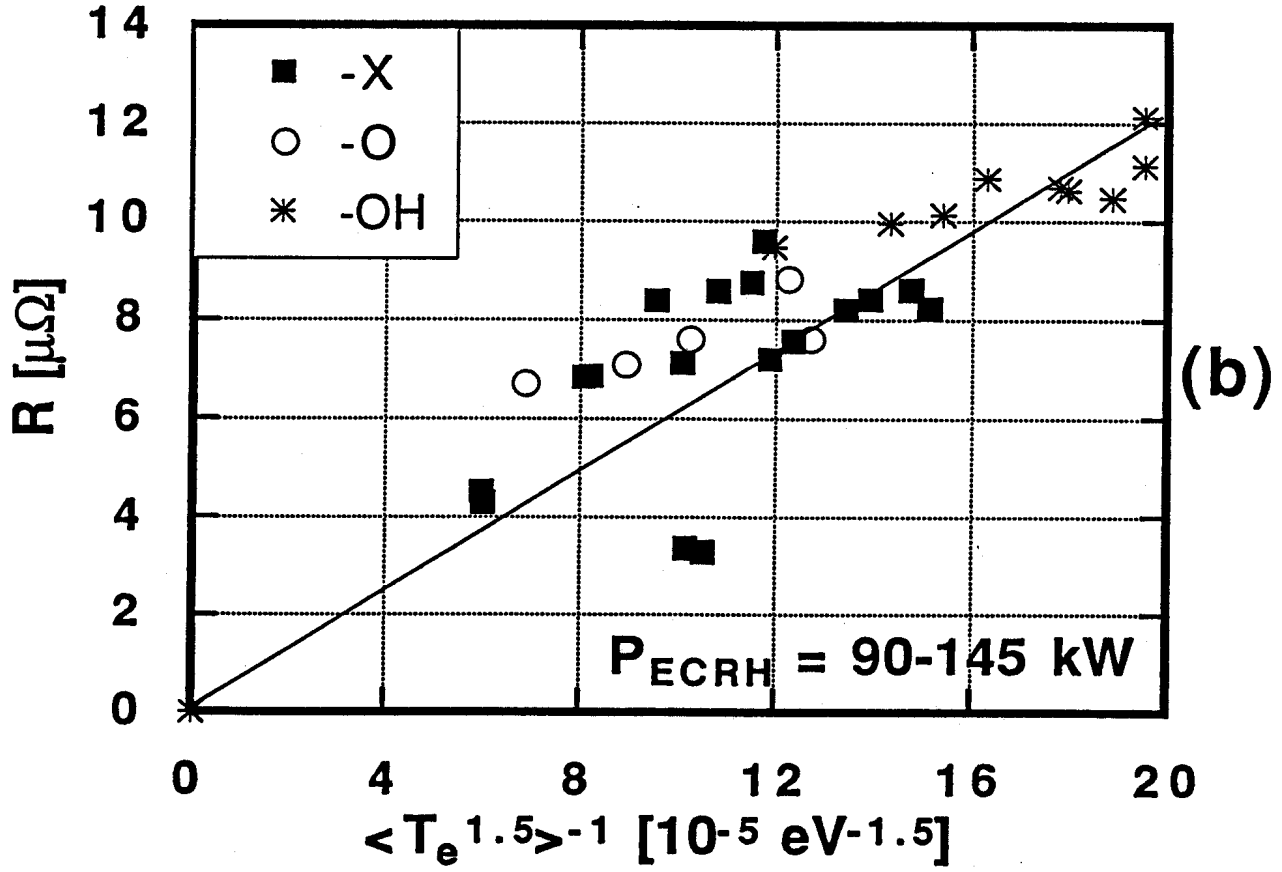
14
12
10
8
6
4
2
0
R [μΩ]
-X
-O
-OH
P_{ECRH} = 90-145 kW
(b)
0
4
8
12
16
20
$<T_e^{1.5}>^{-1}$ [10^{-5} eV$^{-1.5}$]

Figure 9

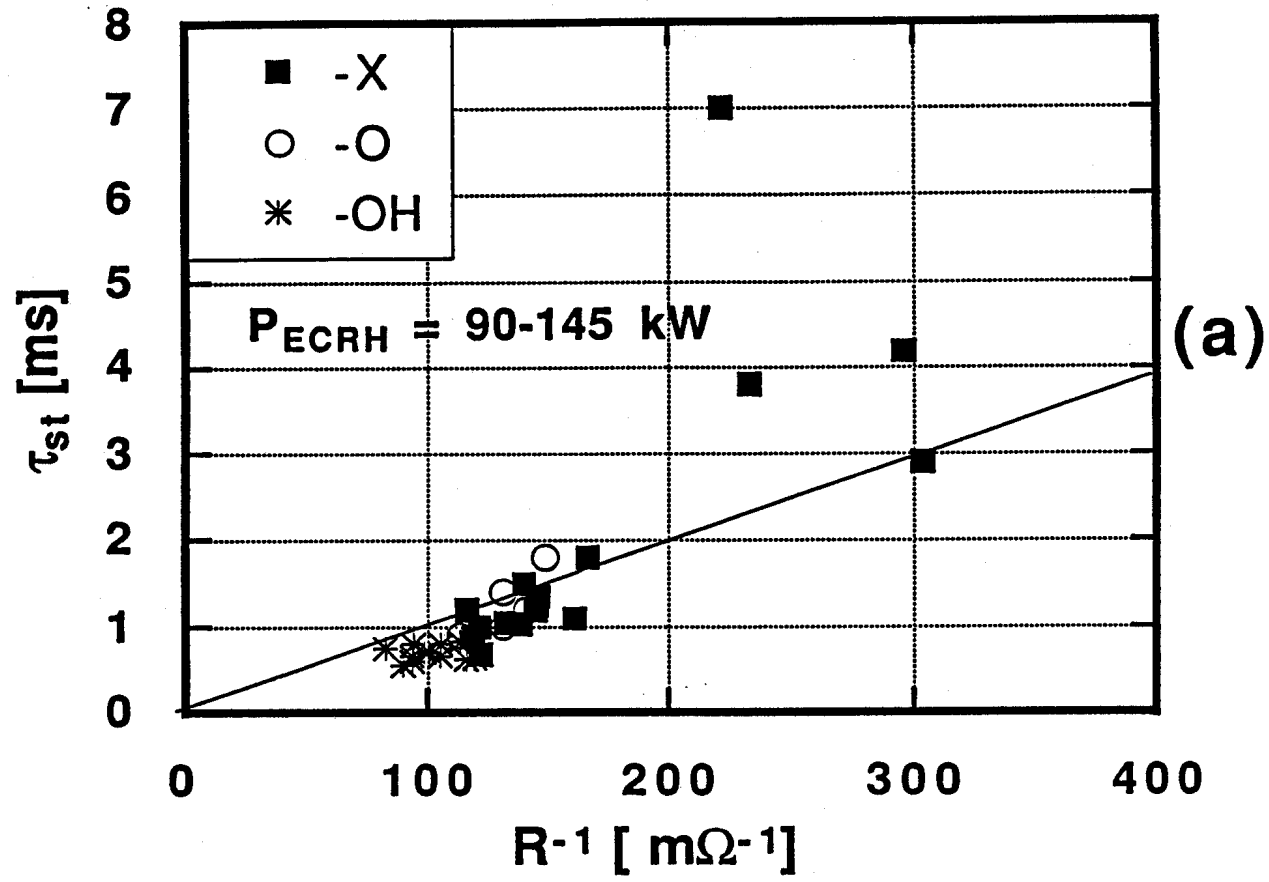
■ -X
○ -O
✳ -OH
P_{ECRH} = 90-145 kW
τ_{st} [ms]
R^{-1} [mΩ^{-1}]
(a)

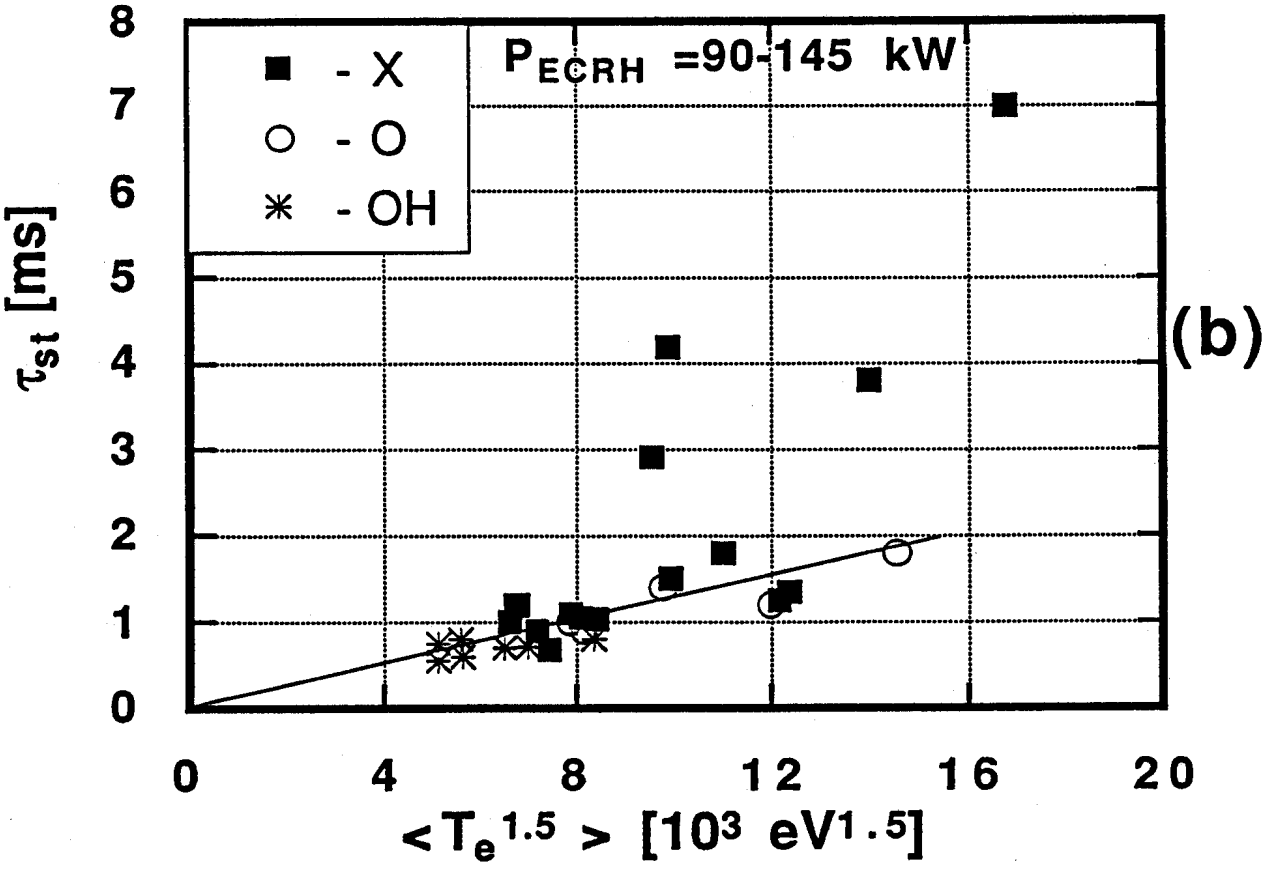
■ - X
○ - O
✳ - OH
P_{ECRH} =90-145 kW
τ_{st} [ms]
$< T_e^{1.5} >$ [10^3 $eV^{1.5}$]
(b)

Figure 10

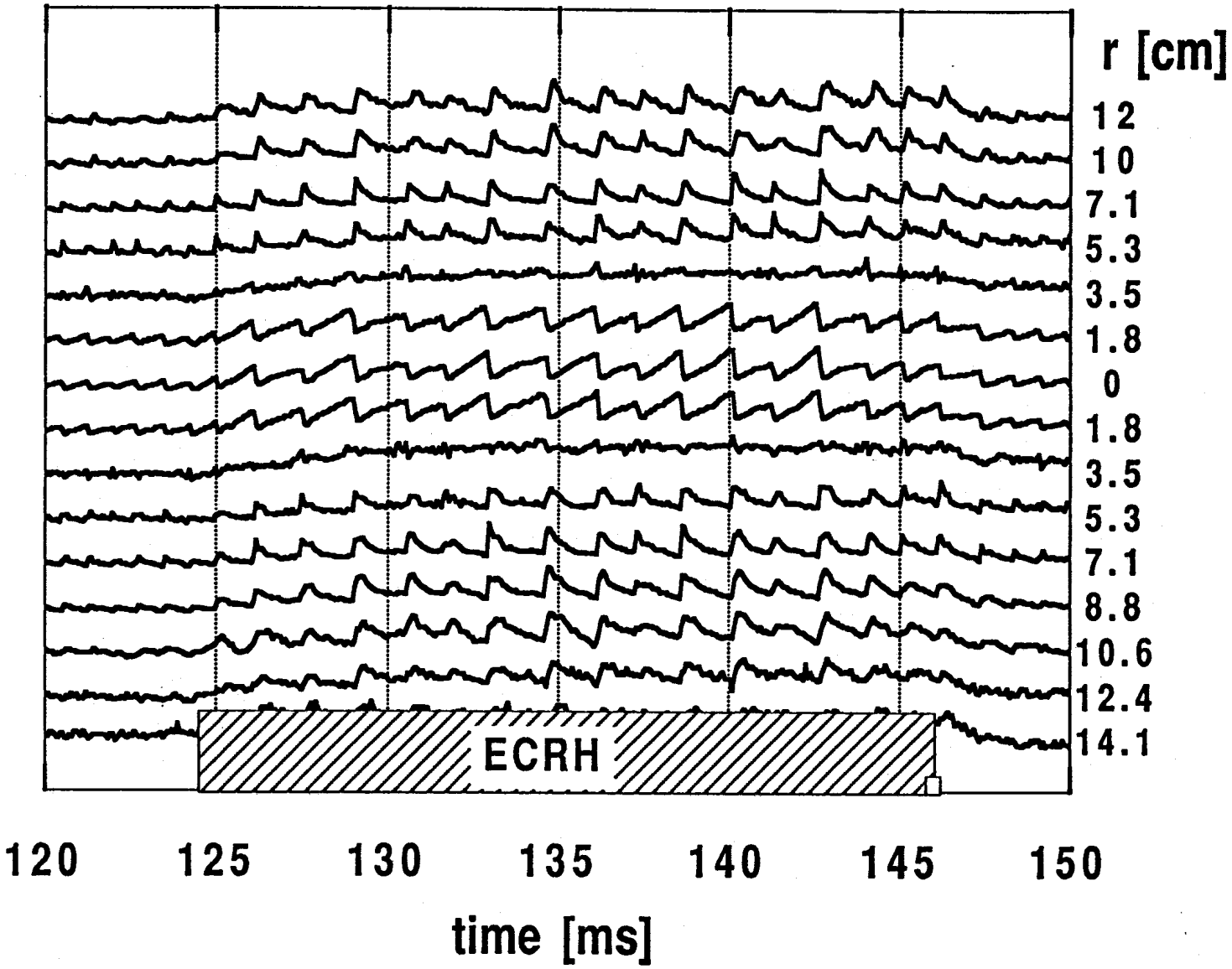
r [cm]
12
10
7.1
5.3
3.5
1.8
0
1.8
3.5
5.3
7.1
8.8
10.6
12.4
14.1
ECRH
120
125
130
135
140
145
150
time [ms]

Figure 11

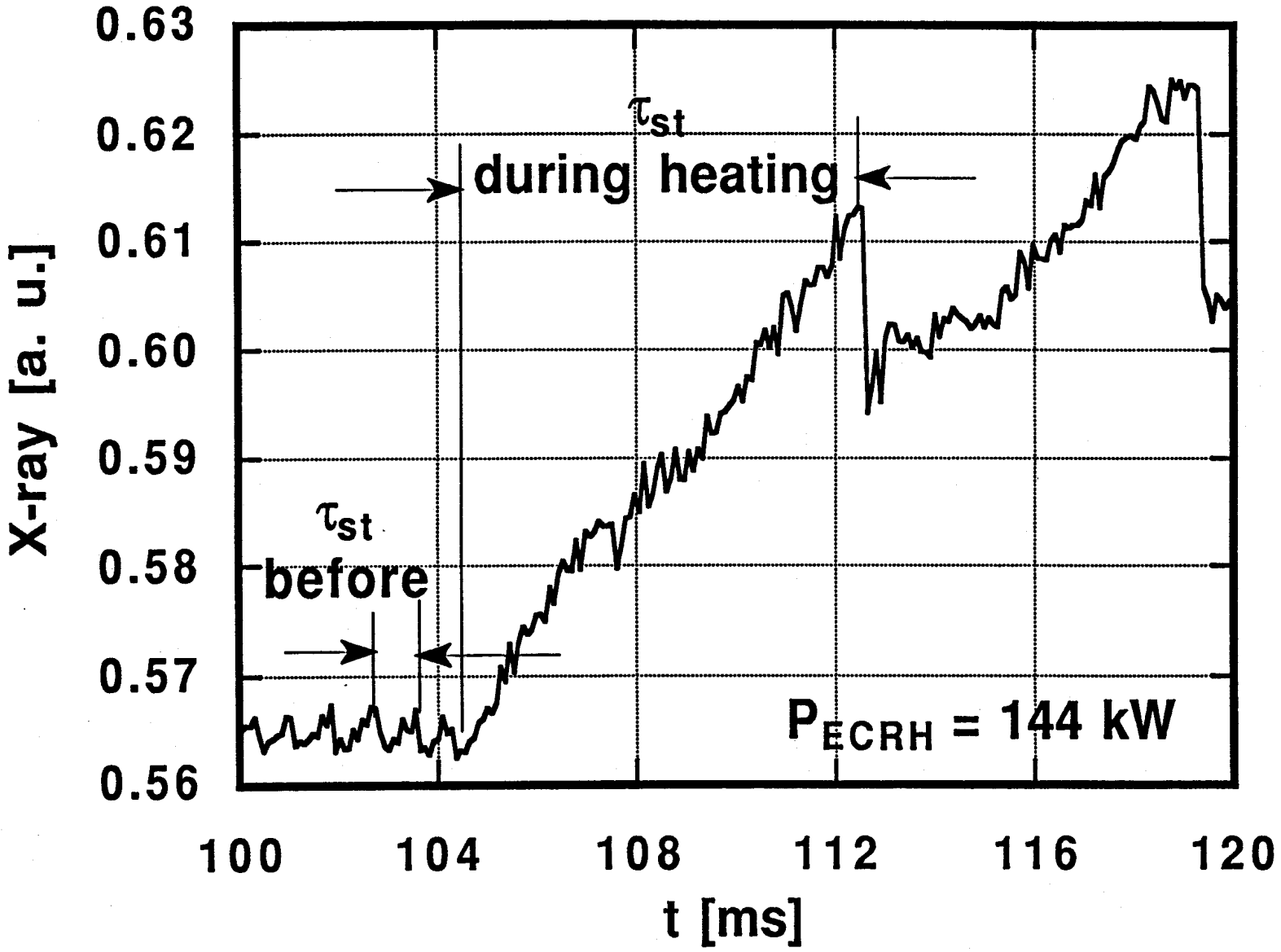
0.63
0.62
0.61
0.60
0.59
0.58
0.57
0.56
X-ray [a. u.]
τ_{st}
during heating
τ_{st}
before
P_{ECRH} = 144 kW
100
104
108
112
116
120
t [ms]

Figure 12

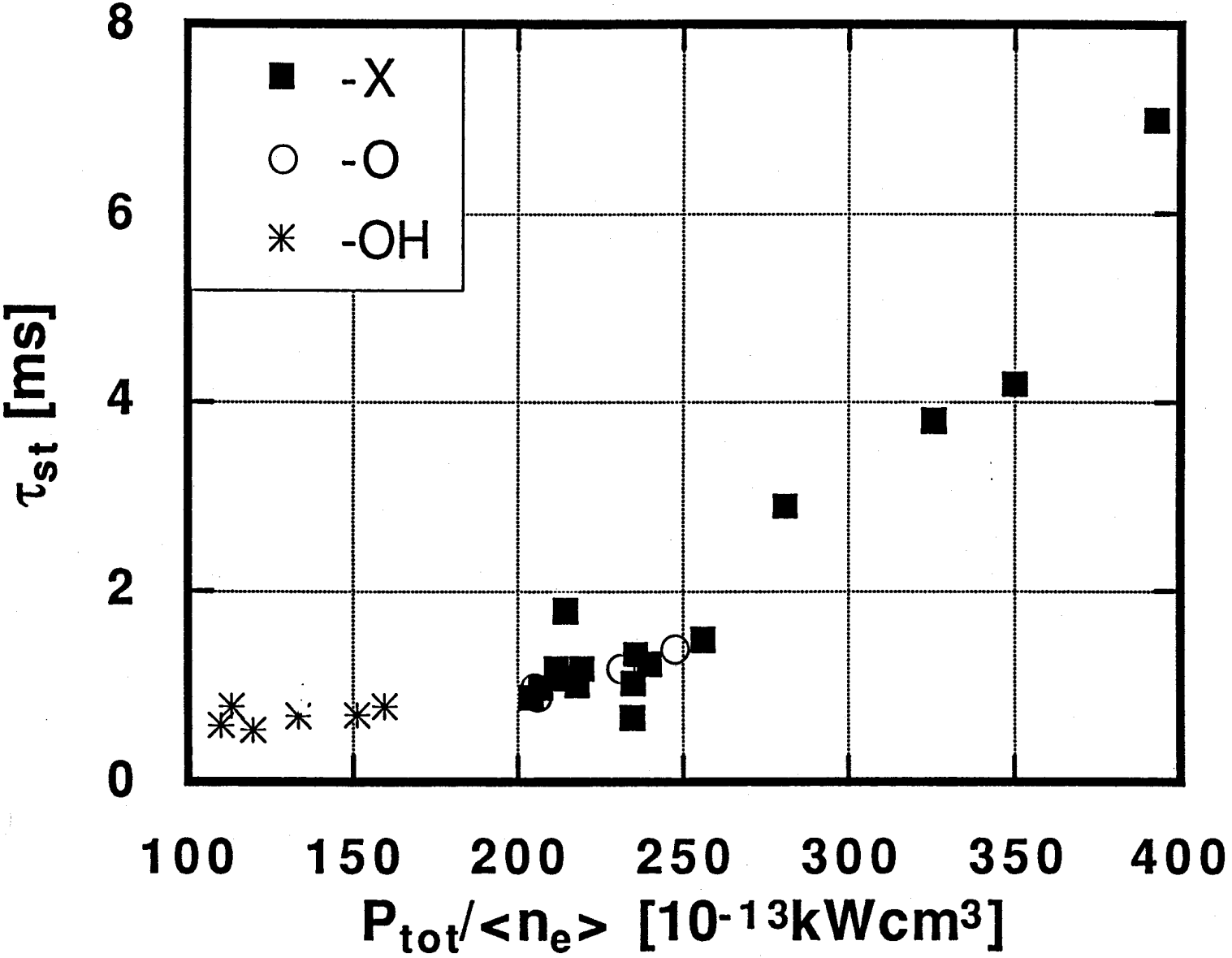
8
6
4
2
0
■ -X
○ -O
✳ -OH
τ_{st} [ms]
100
150
200
250
300
350
400
$P_{tot}/<n_e>$ [10^{-13}kWcm^3]

Figure 13

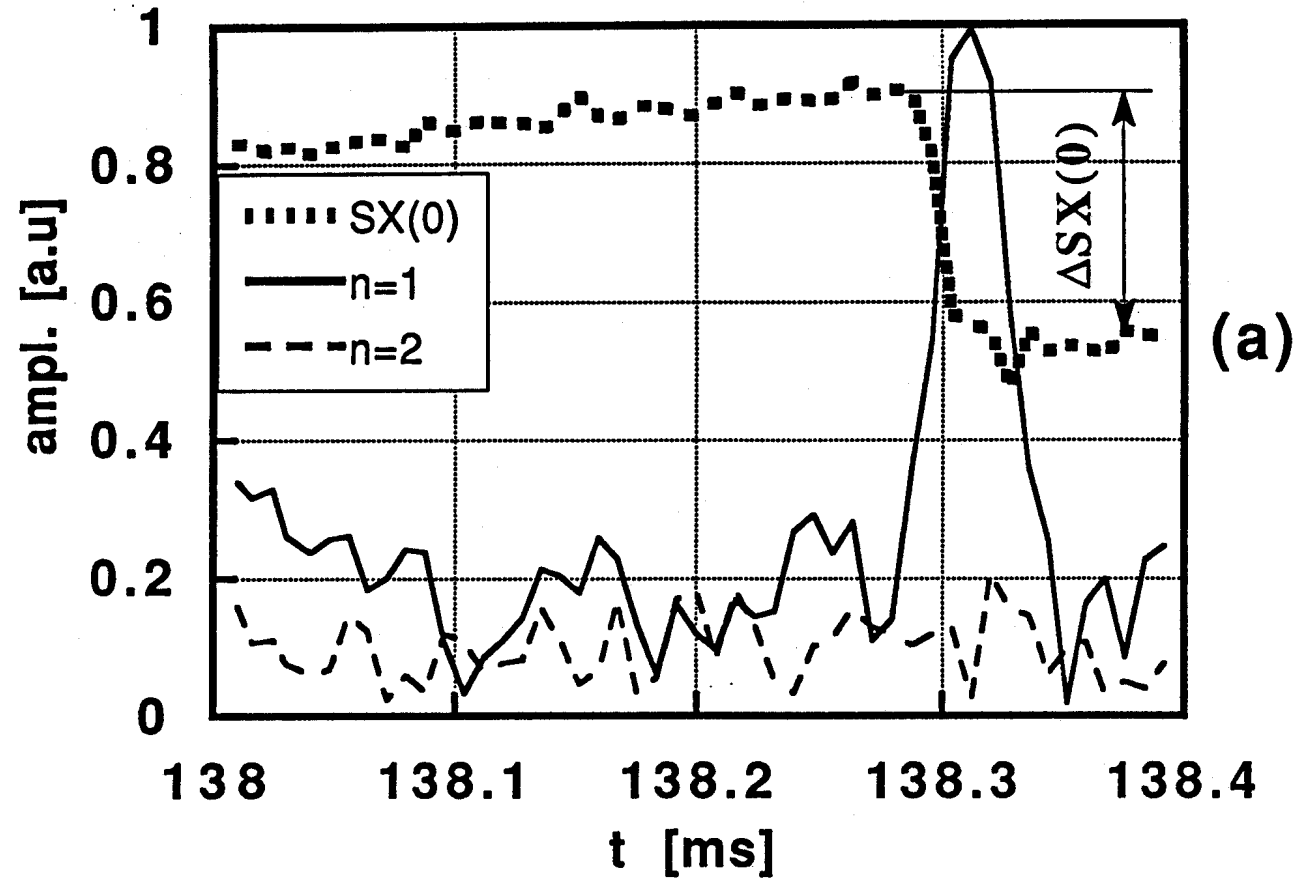
1
0.8
0.6
0.4
0.2
0
ampl. [a.u]
SX(0)
n=1
n=2
ΔSX(0)
(a)
138
138.1
138.2
138.3
138.4
t [ms]

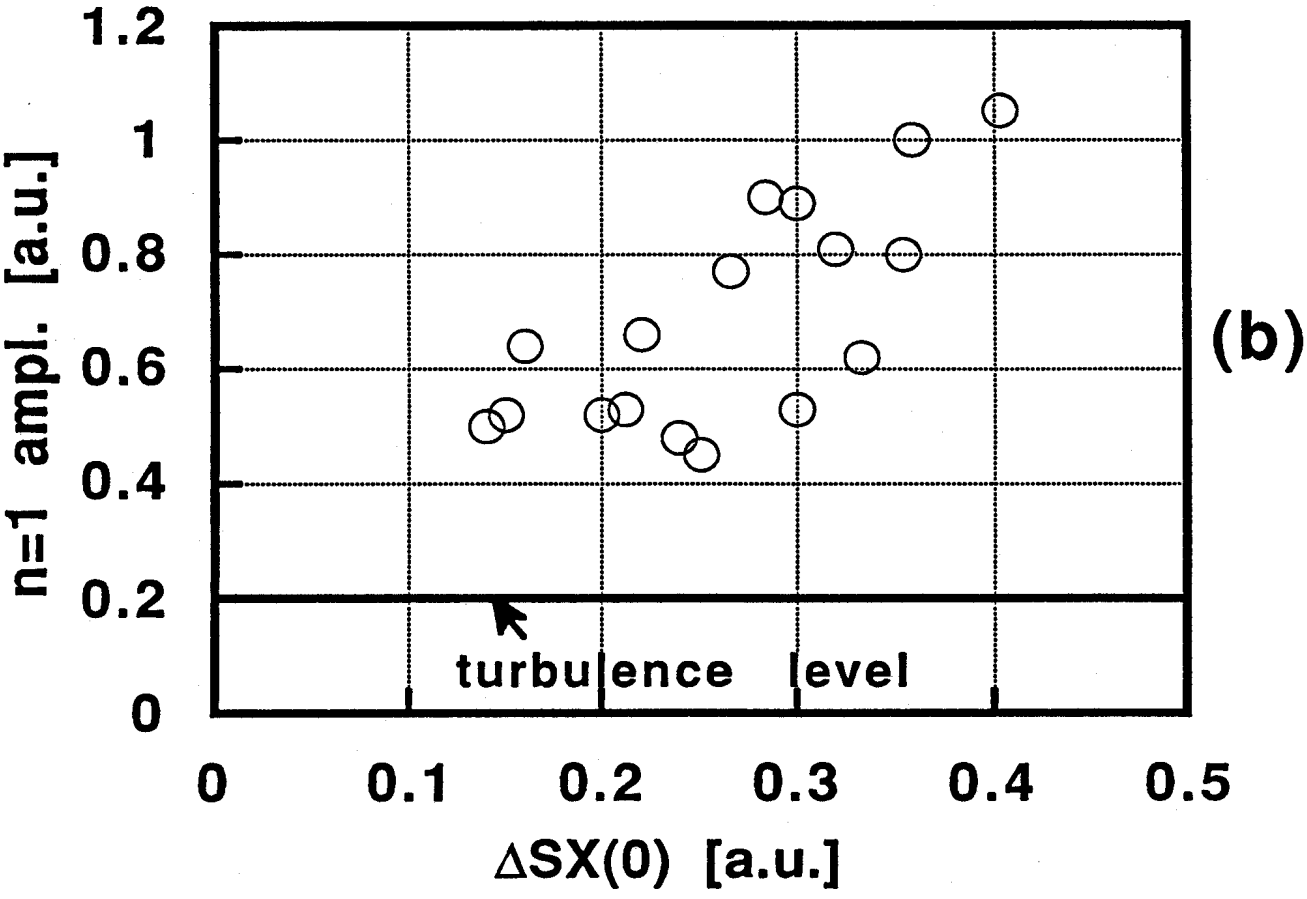
1.2
1
0.8
0.6
0.4
0.2
0
n=1 ampl. [a.u.]
turbulence level
(b)
0
0.1
0.2
0.3
0.4
0.5
ΔSX(0) [a.u.]

Figure 14

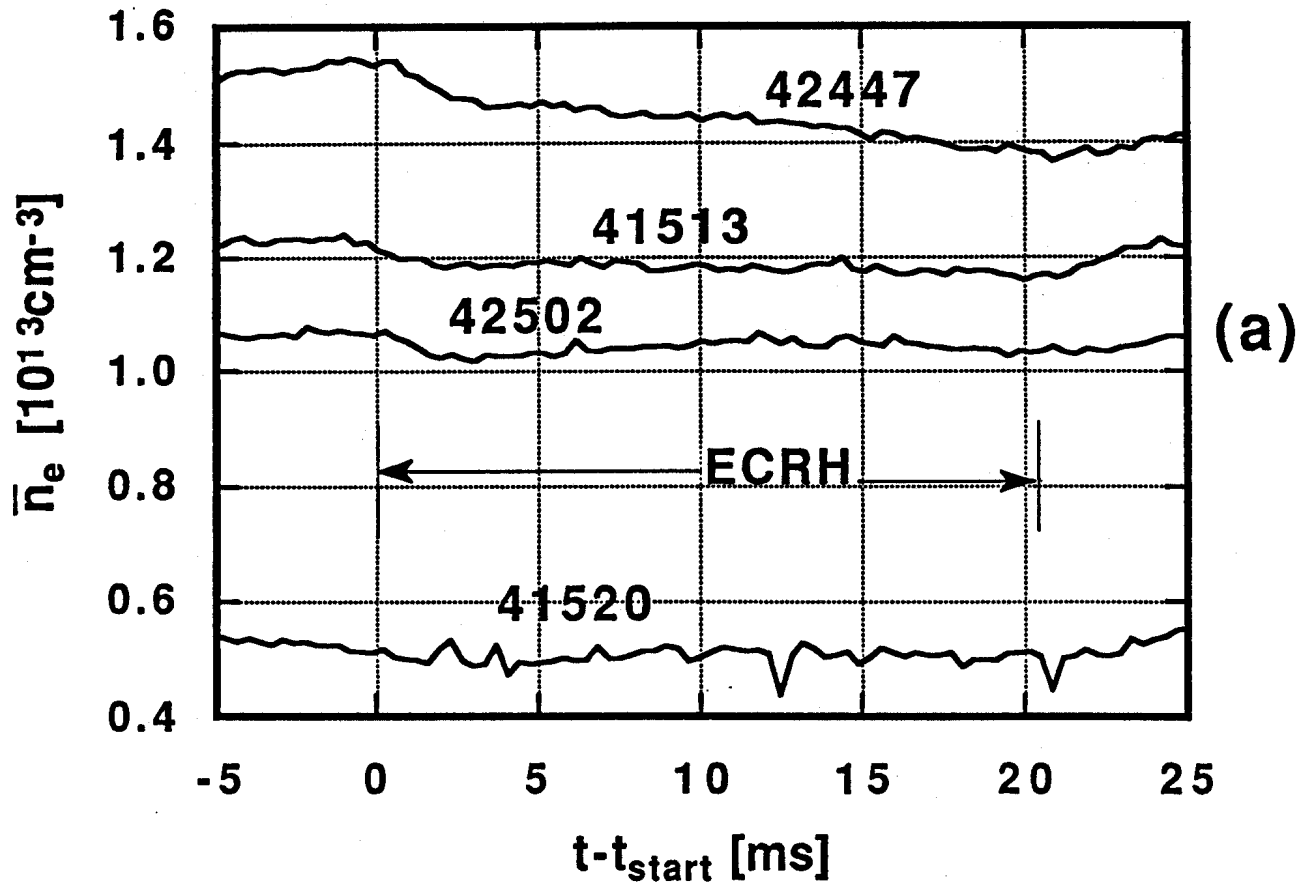
1.6
1.4
1.2
1.0
0.8
0.6
0.4
$\bar{n}_e$ [10^{13}cm^{-3}]
42447
41513
42502
ECRH
41520
(a)
-5
0
5
10
15
20
25
t-t_{start} [ms]

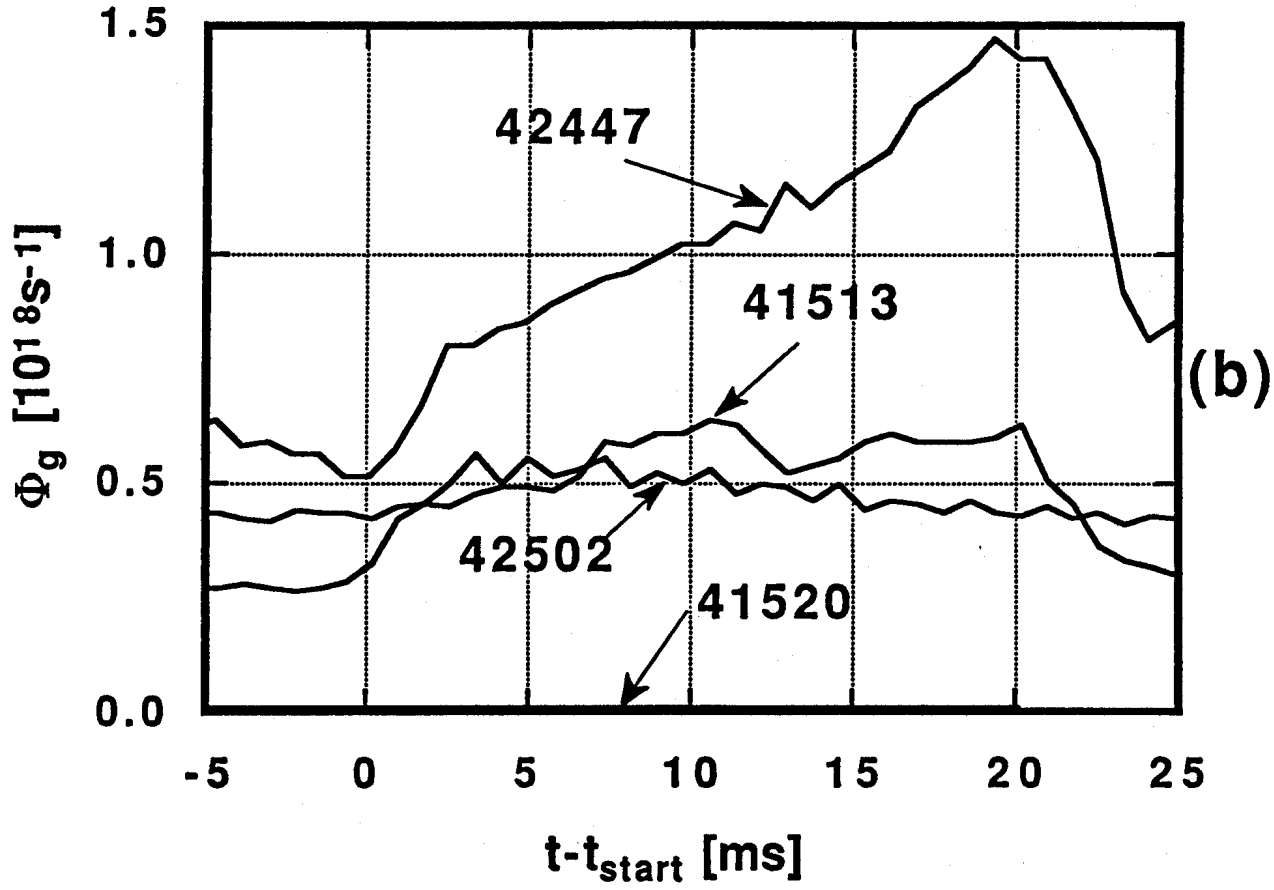
1.5
1.0
0.5
0.0
Φ_g [10^{18}s^{-1}]
42447
41513
42502
41520
(b)
-5
0
5
10
15
20
25
t-t_{start} [ms]

Figure 15

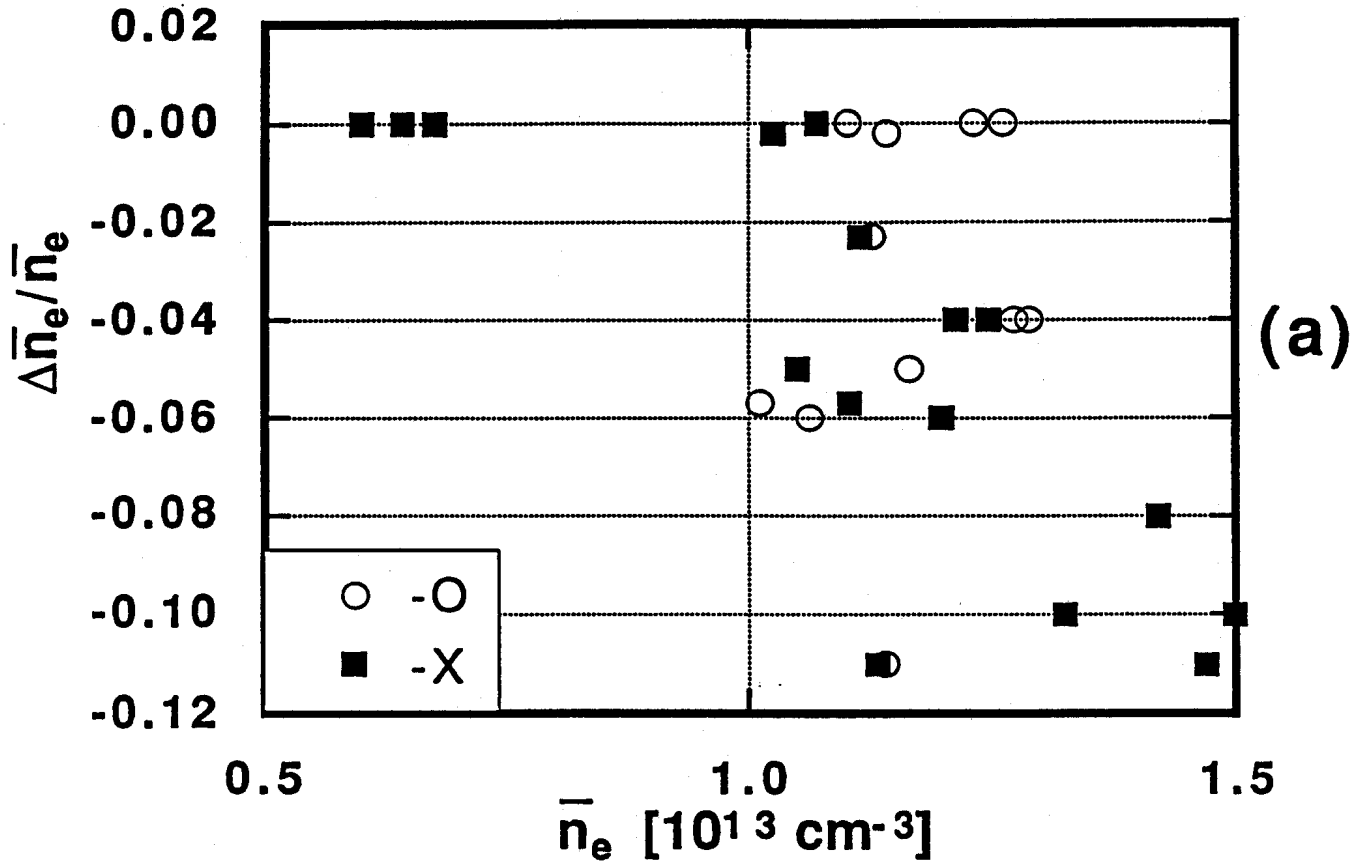
0.02
0.00
-0.02
-0.04
-0.06
-0.08
-0.10
-0.12
$\Delta\bar{n}_e/\bar{n}_e$
-O
-X
(a)
0.5
1.0
1.5
$\bar{n}_e$ [10^{13} cm^{-3}]

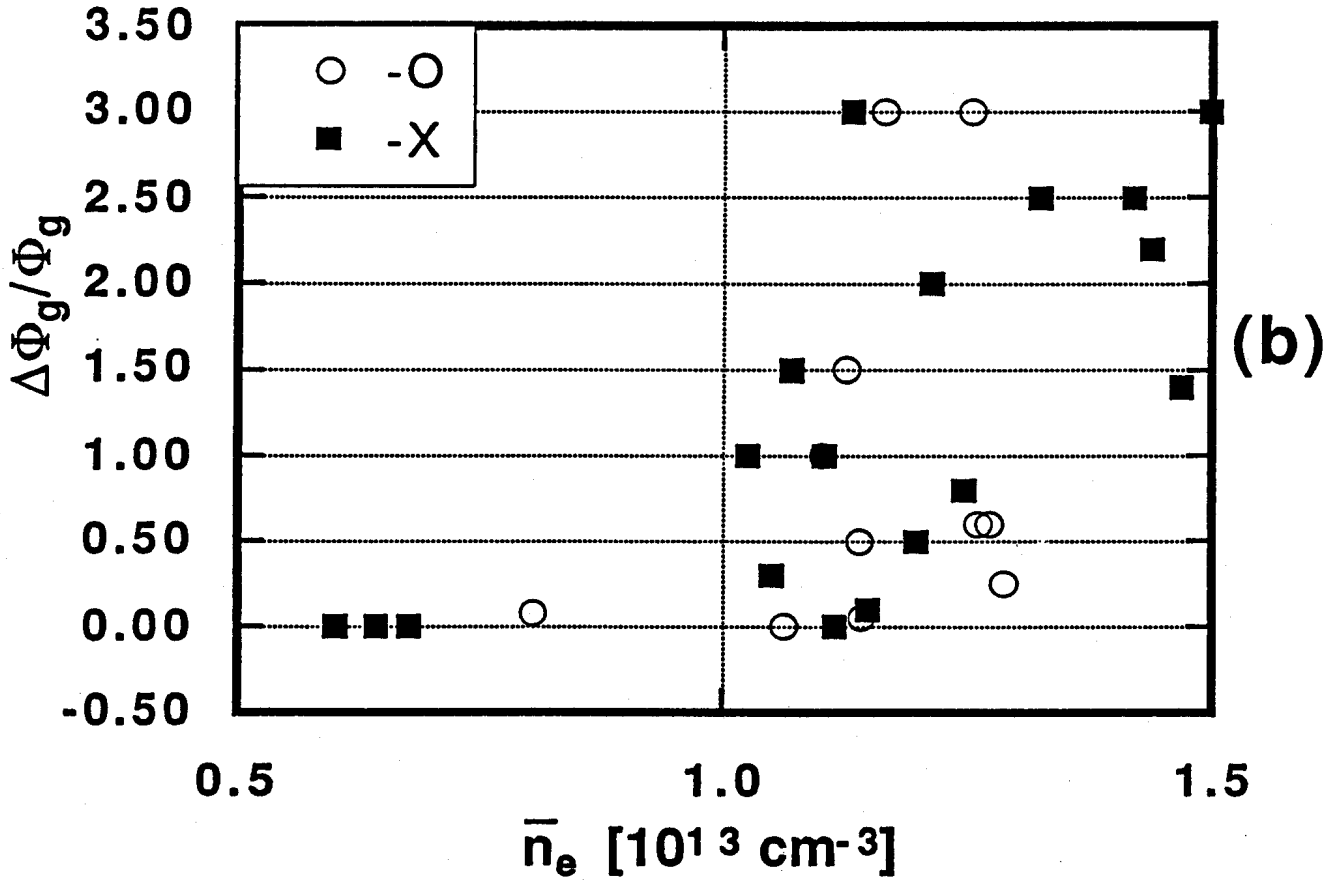
3.50
3.00
2.50
2.00
1.50
1.00
0.50
0.00
-0.50
$\Delta\Phi_g/\Phi_g$
-O
-X
(b)
0.5
1.0
1.5
$\bar{n}_e$ [10^{13} cm^{-3}]

Figure 16

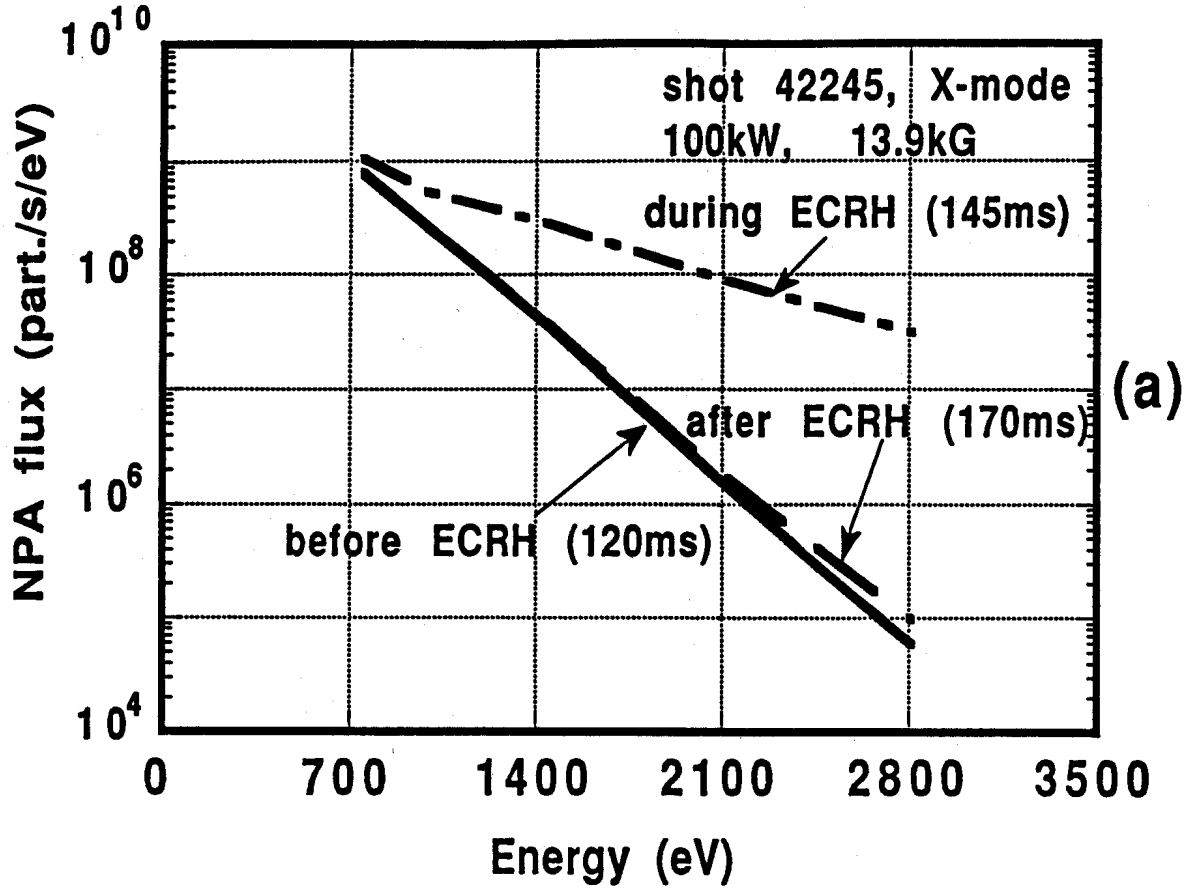
shot 42245, X-mode
100kW, 13.9kG
during ECRH (145ms)
after ECRH (170ms)
before ECRH (120ms)
NPA flux (part./s/eV)
Energy (eV)
(a)

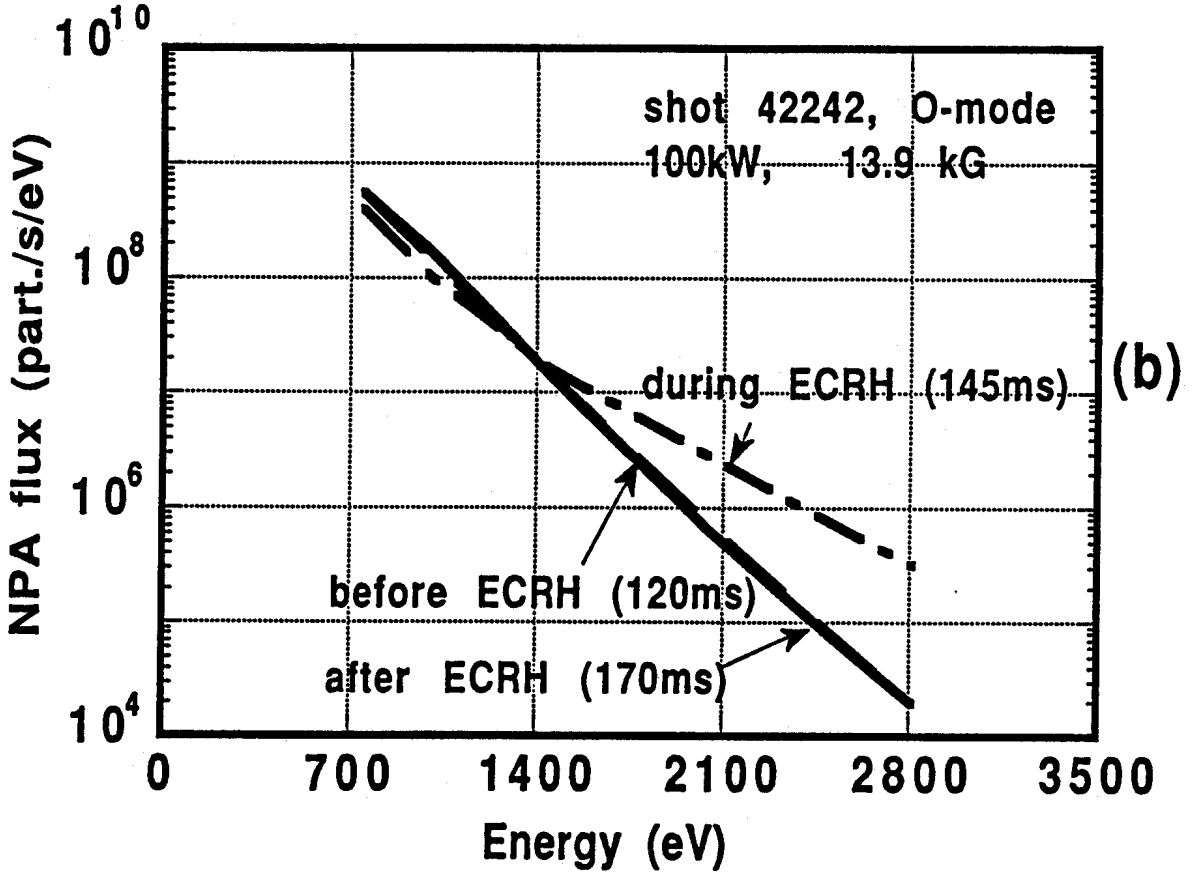
shot 42242, O-mode
100kW, 13.9 kG
during ECRH (145ms)
before ECRH (120ms)
after ECRH (170ms)
NPA flux (part./s/eV)
Energy (eV)
(b)

Figure 17